Politecnico Di Milano

Facoltà di Ingegneria Industriale

Corso di Laurea in

Ingegneria Aeronautica

Ottimizzazione aerodinamica di un velivolo a tre superfici

Aerodynamic optimization of a three surfaces' aircraft

Relatore: Prof. G. Quaranta

Tesi di Laurea di:

Enrico Fabiano Matr. 725291

Anno Accademico 2009 - 2010

Contents

List of Figures

List of Tables

Sommario

In quanto segue si descrive lo sviluppo di un ottimizzatore da utilizzare durante il progetto aerodinamico preliminare di un'ala di un generico velivolo da trasporto transonico. Si presentano inoltre i risultati per l'ottimizzazione di un'ala rigida ed elastica.
Durante il progetto preliminare è necessario poter esplorare quante più soluzioni progettuali possibili nel minor tempo possibile ed a questo scopo sono necessari strumenti a bassa fedeltà veloci e quanto più possibile affidabili. A questo scopo è stata utilizzato il codice a reticolo di vortici AVL la cui esecuzione richiede pochi secondi sui moderni computer di tutti i giorni. L'aerodinamica lineare dei codici a reticolo di voritci, e la loro generalizzazione al regime comprimibile subsonico attraverso la correzione di Prandtl Glauert, non può essere utilizzata in una ottimizzazione transonica a causa dell'eventuale insorgere di urti ed effetti non lineari che non possono essere modellati; a questo scopo è stata sviluppata una procedura di correzione, basata sulla teoria delle striscie, dei dati di AVL tramite polari bidimensionali ottenute con il codice CFD EDGE. Nel caso aeroelastico la struttura è stata modellata in MSC NASTRAN con semplici elementi di trave.
Come riferimento si è preso il velivolo tre superfici X-DIA sviluppato al Politecnico Di Milano: ne è stata ottimizzata la geometria dell'ala utilizzando come variabili lo svergolamento di sette sezioni lungo l'apertura. In tutti i casi si è utilizzata la tecnica delle superfici di risposta, in particolare per l'ottimizzazione rigida è stata utilizzata la tecnica del *gradient enhanced kriging*, mentre nel caso aeroelastico è stato utilizzato la tecnica del *kriging* nella sua formulazione classica. In tutti i casi, tranne l'ottimizzazione aerostrutturale, il *design of experiment* iniziale è stato raffinato con un approccio di ricerca globale dell'ottimo chiamato *Efficient Global Optimization*. Per l'ottimizzazione dell'ala si è seguito un approccio innovativo: anzichè consentire un incremento di momento picchiante per un determinato coefficiente di portanza di progetto l'ala è stata ottimizzata chiedendo che il velivolo sia trimmato in condizioni di crociera per ogni geometria proposta dall'ottimizzatore. Il problema del trim del velivolo è stato affrontato utilizzando tutte le superfici disponibili, con l'obiettivo di ottenere una riduzione complessiva della resistenza di trim rispetto alla configurazione con canard ad incidenza fissa, come nella versione originale dell'X-DIA. Utilizzare sia il canard sia il piano di coda orizzontale complica il problema del trim dal momento che non ne esiste più una soluzione unica; si è pertanto deciso di ricorrere ad una nuova procedura di ottimizzazione, per la quale sono stati considerati diversi algoritmi di ottimizzazione, comprese nuovamente le superfici di risposta e la ricerca diretta tramite un metodo del gradiente. Si è deciso di utilizzare la ricerca diretta principalmente per la sua abilità nel gestire i vincoli e per la sua facilità di implementazione. La sensibilità alla condizione iniziale dell'ottimizzatore non si è dimostrata significativa, essendo le variazioni della funzione obiettivo dell'ordine del *decimillesimo* del coefficiente di resistenza, normalmente espresso in dragcount, e solitamente inferiore suggerendo un insieme di progetto relativamente piatto anche quando fosse utilizzata la correzione transonica di cui si è discusso prima. In sostanza

- l'ottimizzatore aerodinamico propone una geometria per l'ala, una distribuzione di twist

- si procede al trim del velivolo utilizzando il metodo del gradiente
- si valuta il coefficiente di resistenza, corretto per la comprimibilità e la viscosità, del velivolo in equilibrio.

Ovviamente la soluzione ottima sarà quella di minor resistenza, almeno nel caso della sola ottimizzazione aerodinamica.
La correzione di comprimibilità è stata applicata alla sola ala ogni volta che una chiamata di AVL si è resa necessaria, mentre gli effetti di comprimibilità sulle superifici di controllo sono stati modellati tramite la correzione di Prandtl Glauert di cui sopra, questo perchè agli alti numeri di Mach l'impegno delle superfici di controllo è minimo cosicchè esse non risentono di significativi effetti non lineari: in queste condizioni la correzione di Prandtl Glauert può essere utilizzata.
La correzione transonica sviluppata è stata imposta chiedendo che il coefficiente di portanza locale di AVL e di EDGE bidimensionale in quelle sette stazioni utilizzate per l'ottimizzazione aerodinamica sia lo stesso per i due codici, condizione che si può fare verificare tenendo in considerazione l'incidenza indotta ed utilizzando un termine di svergolamento aggiuntivo alle geometrie di AVL. La richiesta condizione di eguaglianza tra i coefficienti di portanza dei due codici è risolta nuovamente attraverso l'imposizione di un problema di ottimizzazione non lineare per la presenza stessa dell'incidenza indotta: questo problema è stato affrontato con le tecniche standard della regressione ai minimi quadrati non lineari.
Una volta che l'uguaglianza tra i coefficienti di portanza è stata soddisfatta è possibile calcolare l'angolo di incidenza effettivo delle sette sezioni ed entrare così nelle polari dei profili per ricavarne resistenza e momento picchiante, da cui ne segue la distribuzione degli stessi lungo l'apertura e, tramite integrazione, i coefficienti globali relativi all'ala. La ricostruzione del coefficiente di resistenza è necessario nella procedura di ottimizzazione aerodinamica, permettendo di introdurre sia il contributo viscoso sia il contributo dell'urto, mentre il coefficiente di momento e la sua distribuzione sono fondamentali sia per affrontare il problema del trim sia per il ciclo aeroelastico.
La natura bidimensionale di questa correzione, ed in generale della teoria delle strisce cui ci si è rifatti, non è in grado di tenere in alcuna considerazione eventuali effetti tridimensionali. Ci si aspetta che questi siano significativi in prossimità dell'estremità alare e molto meno nella parte interna a causa del ridotto angolo di freccia.
I risultati dell'ottimizzazione così ottenuti sono quindi confrontati con verifiche EDGE tridimensionali e saranno tratte conclusioni sulle differenze tra i due modelli.

Abstract

A computational tool to be used early in the wing design phase of a generic transonic transport aircraft has been developed and results for both a rigid and elastic optimization will be presented.
During early design phases runtime is a serious issue so that fast low level code are needed. Here the AVL Vortex Lattice Method has been used throughout the work for it can be run quickly on everyday computers. Being in the transonic regime some sort of correction need to be applied to AVL since it cannot account for the presence of shock waves and Prandtl Glauert theory cannot be relied upon in an optimization environment. A strip-theory-like correction has then been developed using two dimensional transonic CFD data from the EDGE code. Wing structure is modelled in MSC NASTRAN using a classical stick model.
The three surface X-DIA rigid aircraft has been taken as a reference and its main wing has been twist-optimized at seven different spanwise station by means of a gradient enhanced kriging. The original design of experiment is refined by means of the Efficient Global Optimization (EGO) approach. A novel approach to wing optimization has been followed: instead of allowing for a maximum increase in wing pitching moment at design lift coefficient the aircraft is to be trimmed at each design sites. The trim problem is dealt with using all three surfaces, with the objective of reducing trim drag with respect to a fixed canard aircraft as is the original X-DIA aircraft.
Using both canard and horizontal tail adds some complexity to the trim problem since no unique solution exist any more: this issue is addressed setting up another optimization process.
Different optimization strategies has been considered for this purpose including simple kriging, gradient enhanced kriging and a gradient based constrained optimization process which, by the way, turned out to be the most suitable because of its constraints handling capabilities. Trim sensitivity to its initial guess has been considered but it appeared to be of no concern resulting in just one *dragcount*, and usually less, drag difference suggesting a relatively flat design space even when the correction was on.
Consequently this work consists of two nested optimizations:

- the aerodynamic optimization procedure gives a candidate twist distribution
- the aircraft is trimmed with a gradient based method
- the corrected trimmed aircraft drag coefficient is evaluated.

Obviously the optimum twist distribution will be the one with the lowest possible drag, at least for a pure aerodynamic optimization.
Compressibility correction is applied to the main wing only any time an AVL run is needed; control surfaces compressibility effects are handled with the aforementioned Prandtl Glauert theory. At high Mach number control surfaces deflections are small so that no shock is seen on their surfaces and Prandtl Galuert theory works fairly well. Transonic CFD correction is applied requiring that AVL and EDGE lift coefficient at those wing stations used during the aerodynamic optimization is the same taking into account induced incidence by means

of a fictitious twist term. Lift coefficient equality is a non linear problem for the presence of the induced incidence itself and we address it with a non linear least square technique.
Once lift coefficient equality is satisfied one can enter airfoil drag and pitching moment curve using the effective angle of attack to compute drag and pitching moment coefficient distribtution from CFD. Drag reconstruction allows to take shock and viscous drag into account to be used in the overall twist optimizer while the pitching moment is needed in both the trim optimization process and in the jig-1g loop of the flexible wing.
The two dimensional nature of the developed strip-theory correction cannot account for three dimensional effects, that we believe are significant at wing tip and much less at inboard stations because of the low sweep angle.
AVL twist-optimized wing will then be analyzed in a three dimensional CFD computation and results from this two different fidelity model will be compared.

Chapter 1

Descrizione dell'attività

In questo capitolo si propone una breve descrizione del lavoro svolto. Tutti i necessari dettagli e i risultati possono essere trovati nei capitoli a seguire.

1.1 Introduzione

Si può affermare che negli ultimi anni l'ottimizzazione numerica di ali e di ogni parte fondante di un velivolo sia diventata una disciplina a sè stante. Al fine di introdurre il lavoro si cerca qui di fare una breve e non esaustiva descrizione delle diverse fasi di progetto di un aereo, e di un ala in particolare.
Come noto il progetto di un aeroplano è un processo lungo ed iterativo che al giorno d'oggi coinvolge modelli di differente accuratezza in diverse fasi del progetto stesso. Agli inizi del progetto i progettisti hanno solo *un'idea* generale dell'aeroplano e la necessaità di esplorare quante più soluzioni progettuali possibili nel minor tempo possibile richiede che siano utilizzati semplici modelli analitici. Tuttavia, anche in questa fase del progetto è possibile utilizzare tecniche di ottimizzazione numerica al fine di estrarre quante più informazioni possibili dai modelli semplificati a disposizione. Con l'avanzare del progetto si utilizzano modelli sempre più raffinati e computazionalmente onerosi, cosicchè l'uso di calcolatori ad alte prestazioni diventa necessario. Quanto appena detto è poi particolarmente vero per il progetto aerodinamico dell'ala. Una volta che il progetto preliminare e quello di dettaglio sono stati conclusi si procede alla fase produzione.
Con il significativo incremento delle prestazioni anche dei calcolatori di tutti i giorni si è inevitabilmente fatta strada la tentazione di utilizzare i modelli raffinati sin dalle primissime fasi del progetto al fine di diminuire drasticamente il tempo necessario per la vendita[1]. Questa tentazione scontra tuttavia con i comunque lunghissimi tempi di calcolo richiesti dal modelli avanzati e dall'alto livello di dettaglio richiesto dai modelli stessi[2]: una soluzione al problema può quindi essere quella di ricorrere a metodi computazionali che richiedono il minor numero di dettagli pur garantendo la massima accuratezza possibile, in accordo con le ipotesi fatte nella loro deduzione.

[1] Inteso come *time to market*

[2] Si pensi al livello di dettaglio richiesto dalla preparazione della geometria di un'ala per un calcolo CFD

Nell'ambito appena descritto lo scopo del presente lavoro è facilmente intuibile: l'obiettivo è quello di sviluppare uno strumento da poter utilizzare nelle primissime fasi del progetto di un aereo transonico che richieda il minor dettaglio possibile, ma che faccia anche uso degli strumenti più avanzati possibili. In quest'ottica l'aerodinamica è decritta da un codice a reticolo di vortice che sui calcolatori moderni può essere eseguito in pochi secondi. Le nonlinearità caratteristiche dell'aerodinamica transonica richiedono che una correzione sia applicata ai risultati lineari dei metodi a reticolo di vortici: sono state quindi usate soluzioni CFD bidimensionali, che ormai possono essere ottenute velocemente sui *laptop computer* di tutti i giorni, per applicare una correzione ai risultati VLM, simile nel principio alla rinomata teoria delle striscie.
Come configurazione di riferimento si è preso l'innovativo X-DIA. Dal momento che l'X-DIA è stato concepito per esplorare diverse soluzioni aeroelastiche l'aeroelasticità deve essere tenuta in considerazione anche in questo lavoro, e questo è stato fatto utilizzando un economico modello a travi in NASTRAN. L'obiettivo è quello di ottimizzare il velivolo *trimmato* in crociera per la minima resistenza utilizzando come variabili di progetto lo svergolmaneto di sette sezioni. Trattandosi di un velivolo a tre superfici, utilizzate tutte per il trim, il problema dell'equilibrio deve essere affrontato risolvendo un ulteriore problema di ottimizzazione.
Per l'ottimizzazione aerodinamica sono stati abbondantemente utilizzati metodi di approssimazioni quali le superfici di risposta e il kriging, mentre per risolvere il problema del trim si è utilizzato un metodo del gradiente.
I risultati delle ottimizzazioni sono infine stati verificati con calcoli CFD tridimensionali al fine di poter giudicare lo strumento progettato.

1.2 Analisi e ottimizzazione tramite superfici di risposta

Per l'ottimizzazione aerodinamica, e più in generale in tutto il lavoro, sono stati abbondantemente utilizzati dei metodi di approssimazione quali le superifici di risposta e il kriging, sia quello classico sia quello aumentato con il gradiente della funzione approssimata.
Il primo e probabilmente più diffuso metodo di ottimizzazione è quello mediante superifici polinomiali di risposta, i cui coefficienti sono determinati tramite il metodo dei minimi quadrati. Sono metodi molto diffusi, ma sono anche caratterizzati da alcuni svantaggi, in particolare l'incapacità di seguire comportamenti fortemente non lineari della funzione che si sta approssimando. E' noto che il successo della loro approssimazione dipende anche dal *design of experiment* e difettano di una chiara procedura di raffinamento dello stesso.
Alcuni dei problemi appena citati possono essere superati con l'uso del kriging, uno strumento molto di moda negli ultimi anni e che è nato nella geostatistica. Essendo possibile dividere l'approssimazione data dal kriging in un modello medio più una deviazione è intuitivo capire come questo strumento sia in grado di approssimare meglio eventuali comportamenti non lineari. Inoltre, dal momento che si assume che la deviazione dal modello medio sia il frutto di un **processo gaussiano stazionario**, è possibile definire un errore di approssimazione e, ulteriormente, la probabilità di miglioramento at-

tesa rispetto alla attuale migliore osservazione della funzione approssimata. Quest'ultima possibilità rende particolarmente vantaggioso l'uso del kriging e lo svincola dall'iniziale design of experiment, dal momento che è possibile raffinare quest'ultimo ovunque sia massima la probabilità di miglioramento attesa. Sono inoltre state proposte modifiche alla versione originale del kriging, e di particolare rilievo, anche perchè sono state qui utilizzate, sono quelle che prevedono di sfruttare, oltre alla informazioni sulla funzione approssimata, anche quelle sulle sue derivate; in questo caso si parla di *cokriging*, diretto od indiretto a seconda di come si utilizzino le informazioni sulle derivate.

1.3 Procedura di ottimizzazione

Come indicato in precedenza l'obiettivo di questo lavoro è l'ottimizzazione aerodinamica di un'ala transonica. Le variabili di ottimizzazione sono lo svergolamento di sette sezioni lungo l'apertura alare. La funzione obiettivo di questa ottimizzazione è la resistenza globale del velivolo equilibrato che, grazie alla procedura di correzione, è la somma della resistenza indotta e della resistenza dovuta alle non linearità del flusso.
Il velivolo oggetto dell'ottimizzazione è il *Target Aircraft*, una versione ingrandita dell'X-DIA. Questo è un velivolo a tre superifici e si è deciso di utilizzare sia il piano di coda orizzontale sia il canard al fine di trimmare il velivolo. L'uso indipendente delle tre superfici fa si che per affrontare il problema dell'equilibrio del velivolo in crociera sia necessario risolvere un nuovo problema di ottimizzazione, non essendo più valida la procedura tipica descritta nei manuali di meccanica del volo. Una volta che il velivolo è stato trimmato si procede alla costruzione della funzione obiettivo della ottimizzazione aerodinamica, cosicchè il risultato di questa ottimizzazione sarà la resistenza dell'aeroplano in equilibrio.
Ogni volta che sono necessari i coefficienti aerodinamici, sia nel caso del trim sia nel caso dell'ottimizzazione aerodinamica, si applica la procedura di correzione che consiste nel richiedere che la distribuzione in apertura del coefficiente di portanza del codice a reticolo di vortici sia coincidente con la distribuzione di portanza ottenuta dai dati bidimensionali CFD una volta che sia stato tenuto in considerazione l'incidenza indotta. Per soddisfare questa condizione si utilizza un termine di svergolamento fittizio il cui effettivo valore si determina con un'altra procedura di ottimizzazione, utilizzando la tecnica dei minimi quadrati nonlineari.
Nel caso aeroelastico la procedura di correzione è anche utilizzata per determinare i carichi agenti sulla struttura.
Infine si è deciso di includere nella ottimizzazione aerodinamica anche un contributo strutturale, determinato in seguito ad una richiamata ad un fattore di carico pari a $n = 2.5$.

1.4 Risultati dell'ottimizzazione

In primo luogo si è deciso di ottimizzare l'ala isolata del velivolo al fine di prendere confidenza sia con la procedura di correzione implementata sia con il comportamento di un'ala a freccia negativa. Al termine dell'ottimizzazione

l'ala ottimizzata è stata verificata con un calcolo CFD tridimensionale. I risultati ottenuti sono incoraggianti, considerando l'alto livello di approssimazione presente nella procedura sviluppata, anche se i coefficienti aerodinamici sono leggermente sovrastimati.
Nel caso del modello completo, con tutte e tre le superfici, il confronto con l'ala in configurazione originale dimostra un miglioramento di 3 *counts*, ma un'analisi approfondita dimostra anche un design space ragionevolmente piatto. L'analisi della distribuzione di carico tra le tre superifici dimostra che l'ottimizzatore tende a scaricare l'ala e ad impegnare le superific di controllo in maniera leggermente maggiore rispetto alla configurazione originale. Una nuova verifica con un calcolo CFD tridimensionale dimostra ancora una volta la validità dello strumento progettato, anche se in questo caso i coefficienti sono leggermente sottostimati, probabilmente perchè la correzione discussa è stata applicata solo all'ala principale. Analizzando i coefficienti relativi all'ala si possono trarre però le stesse conclusioni tratte per il caso test dell'ala isolata.
Nel caso del velivolo elastico il miglioramento stimato dallo strumento qui progettato è di soli due counts, tuttavia le verifiche ad alta fedeltà confermano questo trend. La distribuzione di svergolamento sotto carico dell'ala elastica coincide ragionevolmente con quella dell'ottimizzazione rigida, con un solo count di differenza tra l'ala rigida e quella flessibile, e questo conferma che effettivamente è stato raggiunto l'ottimo, ottimo piuttosto piatto per giunta dal momento che la distribuzione di twist a scalo è stata leggermente modificata, con riferimento ad esigenze costruttive, rispetto alla proposta originale dell'ottimizzatore.
L'inclusione di un termine strutturale alla funzione obiettivo aerodinamica permette di portare a termine un *trade study* evidenziando esigenze opposte tra aerodinamica e struttura.

1.5 Conclusioni e sviluppi futuri

In questo lavoro è stato presentato lo sviluppo di un ottimizzatore aerodinamico da utilizzare durante le fasi preliminari del progetto. Tutti gli obiettivi attesi sono stati raggiunti. La necessità di disporre di uno strumento rapido e sufficientemente accurato è stata soddisfatta ed è stata ottimizzata l'ala del *Target Aircraft* tenendo in considerazione l'aerodinamica, le strutture e la meecanica del volo.
Il centro di questo lavoro è la procedura di correzione che consente al codice aerodinamico AVL di tenere in debita considerazione le eventuali onde d'urto. Tuttavia, invece di utilizzare AVL in tutto il lavoro si è deciso di sfruttare le sue caratteristiche di linearità attraverso l'uso di tecniche di approssimazione che hanno consentito di poter risolvere il problema dell'ottimizzazione con effettivamente pochi *runs* aerodinamici, riducendo ulteriormente il costo computazionale. Esattamente uno degli obiettivi che ci si era posti inizialmente.
I risultati di questa ottimizzazione sono stati confrontati con calcoli CFD ad alta fedeltà ed è stato trovato un buon accordo tra i due metodi, ma, ciò che è più importante, la procedura sviluppata appare in grado di stimare correttamente le variazioni delle figure di merito tipiche dell'ottimizzazione aerodinamica quando confrontata con gli stessi risultati CFD. Questo ha due maggiori conseguenze:

- lo strumento sviluppato può essere utilizzato nell'ambito del progetto preliminare per esplorare quante più soluzioni possibili con un costo compu-

tazionale minimo

- può essere usato in una ottimizzazione multidisciplinare multifedeltà come modello a bassa fedeltà, riducendo di molto anche il costo complessivo del progetto avanzato. Si suggerisce per il futuro l'utilizzo del *multifidelity kriging*. Nel caso si rimanga in un ambito esclusivamente computazionale si raccomanda l'uso del *gradient enhanced multifidelity kriging*

Lo strumento sviluppato può quindi essere utilizzato sia per equilibrare il velivolo, sia per la sua ottimizzazione in configurazione di crociera: questo ha rappresentato un aspetto caratteristico del presente lavoro, dal momento che il trim del velivolo è più utilizzato per la determinazione dei carichi agenti che non per la valutazione delle performance aerodinamiche. Il confronto con il modello ad alta fedeltà, che pure ha dato buon accordo, come detto sopra, deve essere portato a termine in modo più formale attraverso uno studio di convergenza di griglia per il modello CFD ad alta fedeltà, argomentazione che qui non è stato possibile portare a termine a causa delle limitate risorse computazionali disponibili.
Relativamente ai piccoli incrementi osservati tra la configurazione originale e l'ala ottimizzata si ritiene che siano dovuti alla natura delle variabili utilizzate e al loro limitato numero. In futuro si dovrebbe consentire almeno la variazione della forma dei profili, attraverso opportuna parametrizzazione, ed in questo caso si ritiene che i miglioramenti dell'ottimizzazione saranno significativi.
La distribuzione di portanza ottenuta dall'ottimizzazione aerodinamica tende a caricare maggiormente le estremità alari. Questa caratteristica è comune a tutte le ali a freccia, ma qui si ritiene sia anche dovuta alla natura dell'ala a freccia negativa, come descirtto durante l'analisi dei risultati. Questa distribuzione di portanza è sconsigliabile da un punto di vista della sicurezza del volo perchè tenderà a far stallare prima le estremità, anche se calcoli a bassa velocità non sono stati effettuati. In una futura ottimizzazione si consiglia di tenere in considerazione anche questo aspetto, anche se un vantaggio del velivolo tre superfici è proprio quello di avere il canard: indipendentemente dalla distribuzione di portanza dell'ala se il canard *stallasse* prima dell'ala principale farebbe nascere un momento picchiante in grado di abbassare l'incidenza del velivolo ed allontanare l'ala dalla condizione di stallo, avendo ancora a disposizione il piano di coda orizzontale per il controllo longitudinale.
I risultati dell'ottimizzazione rigida ed elastica dello svergolmento sotto carico di crociera sono ragionevolmente gli stessi a conferma che è stato raggiunto il vero ottimo possibile. In entrambi i casi è stato trovato un *design space* piatto e si ha l'impressione che questo sia dovuto alla procedura di correzione, anche se in letteratura è possibile trovare diverse discussioni riguardo la natura piatta del insieme di progetto aerodinamico.
La superficie di risposta aerostrutturale necessita certamente di ulteriori analisi con l'obiettivo ultimo di costruire il fronte di Pareto, ma in generale gli studi comparativi qui condotti hanno dimostrato che le esigenze aerodinamiche e strutturali sono in contrasto, e il designer deve tenere effettivamente in considerazioni entrambe. In futuro si intende aggiungere anche un contributo relativo alle qualità di volo alla presente ottimizzazione multidisciplinare.
Relativamente alle tecniche di ottimizzazione si è d'accordo con quanto si rinviene facilmente in letteratura. Non esiste un algoritmo di ottimizzazione unico per tutti i problemi. Ciascun problema ha le sue peculiarità che devono essere

tenute in debita considerazione, così come ogni procedura di ottimizzazione presenta i propri vantaggi e svantaggi. In ogni caso si ritiene l'uso delle superfici di risposta più vanataggioso rispetto ai metodi diretti dal momento che forniscono al progettista una maggiore quantità di informazioni che può successivamente essere utilizzata.
Infine i buoni risultati ottenuti sono stati certamente favoriti dalla limitata freccia del *Target Aircraft* cosicchè lo strumento qui sviluppato andrebbe verificato su ali con freccie maggiori. Ci si aspetta un deterioramento dei risultati a causa dei maggiori effetti tridimensionali.
Come obiettivo ultimo ci si pone quello di realizzare questa procedura di ottimizzazione anche con strumenti ad alta fedeltà cercando, comunque, di contenere l'onere computazionale e temporale ricorrendo, ancora, all'uso delle superfici di risposta.

Chapter 2

Introduction: wing optimization

It's safe to state that over the past few years wing optimization has matured to a discipline of its own. A wing - optimization literature search quickly ends up with plenty of papers where the most different approach to the optimization problem are investigated. Here I'll try to sort things out a bit in order to set the stage for the work to be described later.
As well known aircraft design is a long iterative process involving different fidelity models at different design phases. At the beginning of the design process designers just have a basic idea of the overall aircraft so that simple analytical model as those described in [47] are needed. Even at this stage, Mason [8] and then Raymer [47, 13] shown that one can use optimization procedure to enhance its design. As the design keeps going aircraft models get more and more refined and this is true for the wing too. During these advanced phases high speed computers are needed because of the time consuming nature of aircraft models simulations. Focusing on the aerodynamic design of the wing, in the past designers chose main wing parameters based on experience, nowadays it's common to rely once more upon optimization procedure, as thoroughly described by Jameson in [32]. Once the whole airplane has gone through this detailed design phase it is supposed to go into production.
But with the wide spread of high speed personal computers the temptation, and maybe the ultimate long term goal, is that of running expensive and detailed simulation since the beginning of the design phase with the underlying idea that the sooner one works on detailed models the shorter will be the time to market. Especially with wing design CFD applications in mind, the use of detailed models since the beginning looks weird at least; even not considering run time issues associated with CFD simulations the need for a detailed geometrical description CFD has makes it an unviable option at the beginning of the design process. What one can try to do, while still holding on the idea of using computational methods in the early stage of the design process, is to rely on those methods that require as few geometrical details as possible while retaining the most possible accurate flowfield description keeping run time issues away.
Things get even worse when there's the need to consider structural elastic effects, something common nowadays because high speed aircraft are usually character-

ized by very flexible wings.
With the above picture in mind the aim of the present work is easily set: to develop a fast tool to be used to help the design of a transonic aircraft using as little geometrical detail as possible, while heavily relying on the highest level computational methods available. As stated above, traditionally during preliminary designs simple analytical formulae were used, today however even laptop computer can run simple aerodynamics codes, as a vortex lattice method, in a couple of seconds so that their power can be fully exploited. Being in the transonic regime however means that shock waves will most likely be present. Indeed the goal of a pure aerodynamic optimization is a shock-free wing, and since these features can only be captured by an advanced CFD methods we need a way to make the VLM feel the shocks. Since our aim is to keep the computational cost down we will compute 2D airfoil CFD solutions and apply a strip-theory like correction to the bulk VLM results.
As the reference configuration aircraft we take the innovative X-DIA aircraft: it's innovative because it's a three surface aircraft, intended to take advantage of the presence of both the canard and the horizontal tail to reduce trim drag, and because it's exploit some unique aeroelastic concept [49, 2, 48], so that aeroelasticity need to be taken into account. To do this we will be using a cheap beam-like finite element model that can be run quickly on everyday computers.
Our main goal is to optimize wing's twist for drag minimization purposes: usually wing optimization is performed on a isolated wing model, or even on a whole airplane model taking into account trim issue only by specifying a pitch moment constraint [32]. While this is certainly the most common approach there's no gaurantee that this twist optimization process will yeld the best possible trimmed wing. Besides, we had the canard to keep into account, considering that while it should help in reducing trim drag it will certainly affect the aerodynamic of the main wing: we then came up with an innovative procedure to optimize the wing. At every twist configuration to be evaluated the optimizer need to solve the trim problem so that the optimized wing will really be the best possible wing in cruise. However, we are dealing with a three surface aircraft and to trim the aircraft we need to set up another optimization routine, so that we have two nested optimization: the aerodynamic optimization routine gives a candidate configuration, and once the trim optimization routine manage to trim the aicraft we can proceed to aerodynamic or aerostructural cost function evaluation. Results achieved this way will then be checked with a couple of CFD runs as the final validation of the method.
We heavily relied on metamodeling technique, both regressing response surface and interpolating techniques such as the kriging: rigid twist optimization is performed with a gradient enhanced kriging, while aerelastic wing optimization is operated with a traditional kriging. Initial DOEs are sistematycally refined by means of the expected improvement approach in the rigid case while for the aeroelastic wing we used a large sampling plan of 750 design sites: this allowed us to achieve a global optimum according to our specified cost function. The trim problem is dealt with using a gradient based algorithm: local convergence may be an issue here, but it turned out it wasn't, suggesting a flat design space.
This work is structured as follows: the next chapter, chapter three, will be spent on pure theoretical aspects of surrogate based analysis and optimization, chapter four will go specific on the procedure used in the aeroelastic optimization, mainly describing the transonic correction procedure. Chapter five will present

applications with **rigid** and **aeroelastic** optimization results. Finally in chapter six we'll draw conclusions and investigate possibile future development.

Chapter 3

Surrogate based analysis and optimization

In this chapter we are going in some of the mathematical details of those surrogate methods used in this work. What follow is by no means a thorough review of metamodeling techniques and applications, neither it is supposed to be exahustive with respect to mathemathical details and derivations.
In the first section a review of the most meaningful literature is given, then metamodeling techniques will be presented.

3.1 Literature review

When first facing the subject of optimization one can certainly get confused by the amount of literature on the subject.
Just to scratch the surface of response surface methods and metamodeling one should consult the excellent work from Forrester, Sobester and Keane [35]. There the reader can find a general picture of metamodeling, including design of experiment, regressing response surface, Radial Basis Function, kriging methods and support vector regression, with the emphasis on the kriging and its various aspect. Close to the book goes the paper from the same authors [3] and the works of Queipo et al. [43]. Especially in [3] one get the idea that in the aerospace field the most use metamodeling techniques are response surface and kriging methods. This idea is further developed in Giunta [1], where the author compares regressing against interpolating metamodels, and in Simpson et al. [52] where a multidisciplinary optimization environment is taken into account. Application of response surface methods to transonic aerodynamic design can be found in the work from Kim et al. [22] and in that from Mason et al [50] regarding the supersonic regime.
A thorough description of the kriging as applied to the aerospace industry can be found in the work from Booker [9] where an interesting discussion on the initial DOE can also be found. Since that plenty of work regarding kriging application to aerodynamic or multidisciplinary design can be found in the literature. To name just a few there's the work of Chiba [33], that of Keane [36] and the one of Kroo et al. [15]. In all of these work the reader can find anything from simple application of the basic kriging to the multifidelity kriging. Works from Alonso

et al [11], Mavriplis et al. [54] and Laurenceau et al. [27, 28] deals with the powerful gradient and hessian enhanced kriging. A compulsory reference here, because of the expected improvement approach used later, is also the work of Jones et al [14]. Finally we'd like to note that all the surrogates used in this work have been handled with the powerful MatLab `Surrogates Toolbox` from Viana [53].
Changing the subject to the most common direct optimization methods one can find a very good review with applications in the work from Keane et al [44]. There one can find a description of most of the methods used here, either global or local; an intresting description in global optimization methods applied to multidisciplinary optimization can also be found in Hajela [18]. Many application of gradient based methods with the adjoint method can be found in most jobs from Jameson, e.g. [31, 23, 24]. Their details will not be dealt with here.

3.2 Metamodeling techniques

Different metamodeling techniques aims at cheaply simulate the behaviour of an expensive engineering black box function. Let's say here that $f(\mathbf{x})$ is the expensive k-variable continuous black box function that we want to simulate, so that $\mathbf{x} \in D \subset R^k$. From now on D will be referred as the design space. Beyond continuity we can grasp at the function only by means of discrete samples

$$y(\mathbf{x}_i) = f(\mathbf{x}_i) \quad i = 1 \dots n_s$$

that are expensive to run and therefore need to be handled with care, n_s being the number of samples. Once the set $(\mathbf{x}_i, y(\mathbf{x}_i))$ has been gathered we will build up an inexpensive approximation $\hat{f}(\mathbf{x})$ to the true function $f(\mathbf{x})$. Different metamodeling techniques differ in the way $\hat{f}(\mathbf{x})$ is obtained.
There are many ways to define the initial set $(\mathbf{x_i}, y(\mathbf{x_i}))$, called the *sampling plan*: full factorial design, latin hypercube, orthogonal arrays and many other. While it is known that the goodness of fit of the response surface depends on the initial sampling plan here only latin hypercube sampling has been used because functions to be fitted were either simple function, such as hyperplane or hyperparabola, or because after the initial sampling plan some sort of error based refinment is used. Description of how to build a latin hypercube can be found in [35] and in the literature there referenced, while a review of some of the available design of experiment technique can be found in [43].

3.2.1 Polynomial response surface methods

Polynomials response surface methods are probably the most widely used form of surrogate model. They develop the approximation model by fitting the sample data using a least square regression technique. The true response can be written in the following form:

$$y(\mathbf{x}) = f(\mathbf{x}) + \epsilon \tag{3.1}$$

being $f(\mathbf{x})$ the unknown response function and ϵ a random error. Polynomial approximation of equation 3.1 at sampled locations can be written as

$$y_i = \sum_{j=0}^{m} \beta_j x_i^j + \epsilon_i \qquad i = 1, ..., n_s \tag{3.2}$$

or in matrix form as

$$\mathbf{y} = \mathbf{X}\beta + \epsilon \tag{3.3}$$

being $\mathbf{y} = [y_1, ..., y_{n_s}]^T$, and

$$\mathbf{X} = \begin{bmatrix} 1 & x_1^1 & x_1^2 & \dots & x_1^m \\ 1 & x_2^1 & x_2^2 & \dots & x_2^m \\ \vdots & \vdots & \vdots & \vdots & \vdots \\ 1 & x_n^1 & x_n^2 & \dots & x_n^m \end{bmatrix} \tag{3.4}$$

β is the $(m \times 1)$ regression coefficients' vector, ϵ is an $(n_s \times 1)$ vector of random errors and m the order of the polynomial.
The vector of least squares estimator is determined by minimizing the classical quadratic figure of merit

$$L = \sum_{i=1}^{n_s} \epsilon_i^2 = (\mathbf{y} - \mathbf{X}\beta)^T (\mathbf{y} - \mathbf{X}\beta) \tag{3.5}$$

so that

$$\mathbf{b} = \left(\mathbf{X^T X}\right)^{-1} \mathbf{X}^T \mathbf{y} \tag{3.6}$$

A questions remains about the order of the polynomial to be used, indeed some authors suggest to determine the appropriate order using a statistical approach. No matter what the estimated order is, using high order polynomial might lead to data over-fitting and unwanted oscillations, the well known Gibbs phenomenon.
Some authors also argue that polynomial response surface model are not well suited to capture non-linear, multi-modal, multi-dimensional design space such as those encountered in engineering design even though they still prove useful when parameters' range is limited and when dealing with a low dimensions design space; while this might be true when considering general engineering function, in the case of aerodynamics optimizations convergence to local minima, as that eventually assured by low degree polynomials response surface, should not be considered as an issue. Indeed classical gradient based optimization methods used for these kinds of problems converge always to the same minimum, as shwon by Jameson [23, 24, 31, 6, 32, 4]. Indeed, many works can be found were polynomial response surface methods are used in transonic aerodynamic optimization, such as reference [5]. One serious drawback might be the dependence on the initial sampling plan and the lack of a clear-cut infill point strategy. This matter will be addressed later while discussing the efficient global optimization approach.
An advantage of polynomial response surfaces is the ability to quickly identify the effect of each variable in the design space from regressing equation 3.2, a very quick model fitting process and response evaluation, and the ability to yeld an equation for the approximated function.
In this work up to second order polynomial response surface have been used.

3.3 The kriging method

The kriging method has its origin in geostatistics and has been first applied to engineering design by Sacks et al. [30]. Since that pioneering work a lot of

kriging variants have been proposed, the most famous are the multifidelity and the gradient enhanced kriging. We will provide details only for those kriging variants used here, starting from the simple kriging from Sacks and Booker [9, 30].

3.3.1 Simple Kriging

While still in the framework of function approximation the kriging technique uses a two component model written as

$$y(\mathbf{x}) = f(\mathbf{x}) + Z(\mathbf{x}) \tag{3.7}$$

$f(\mathbf{x})$ being a global underlying model, or mean model, and $Z(\mathbf{x})$ is the realization of a **stationary gaussian random process** that creates a localized deviation from the mean model; its covariance matrix is

$$Cov\left(y\left(\mathbf{x}_i\right), y\left(\mathbf{x}_j\right)\right) = \sigma^2 \mathbf{R}\left[R(\mathbf{x}_i, \mathbf{x}_j)\right] \tag{3.8}$$

where $\mathbf{R}$ is the correlation matrix obtained computing a user specified correlation function $R(\mathbf{x}_i, \mathbf{x}_j)$ between any two sampled data points $\mathbf{x}_i$ and $\mathbf{x}_j$.
We'll leave the correlation function aside for a while to get the whole picture of the kriging method.
Traditionally the mean model is a constant, but this is not a constraint, indeed in this work up to second order polynomial mean models have been used. For the purpose of the following discussion let us consider a constant mean model. In this case $f(\mathbf{x}) = \beta$, so that equation 3.7 is

$$y(\mathbf{x}) = \beta + Z(\mathbf{x}) \tag{3.9}$$

and the estimated model of equation 3.9 is

$$\hat{\mathbf{y}} = \hat{\beta} + \mathbf{r}^T(\mathbf{x})\mathbf{R}^{-1}\left(\mathbf{y} - \mathbf{f}\hat{\beta}\right) \tag{3.10}$$

$\hat{\mathbf{y}}$ is the $(n_s \times 1)$ column vector of response data and $\mathbf{f}$ is an $(n_s \times 1)$ column vector filled with ones.
There's one last term from equation 3.10 that need to be specified and that is the vector $\mathbf{r}(\mathbf{x})$ which is the correlation vector between $\mathbf{x}$ and the sampled data points, namely

$$\mathbf{r}^T(\mathbf{x}) = \left[R(\mathbf{x}, \mathbf{x}_1), R(\mathbf{x}, \mathbf{x}_2), ..., R(\mathbf{x}, \mathbf{x}_{n_s})\right]^T \tag{3.11}$$

The value for $\hat{\beta}$ comes from a generalized least square solution

$$\hat{\beta} = \left(\mathbf{f}^T\mathbf{R}^{-1}\mathbf{f}\right)^{-1}\mathbf{f}^T\mathbf{R}^{-1}\mathbf{y} \tag{3.12}$$

Basically, chosen the correlation function, one can evaluate the correlation vector at a given point $\mathbf{r}(\mathbf{x})$ and $\hat{\beta}$ and in this way compute the kriging approximation to the true unknown function. As stated above the correlation matrix $\mathbf{R}(\mathbf{x}_i, \mathbf{x}_j)$ is evaluated chosing a correlation function. There exist many correlation functions and in principle one can use any continuous function, but in practice the most

used are Gaussian exponential[1]

$$R(\mathbf{x}_i, \mathbf{x}_j) = \exp\left[-\sum_{t=1}^{k} \theta_t |\mathbf{x}_{i_t} - \mathbf{x}_{j_t}|^2\right] \tag{3.13}$$

and spline function

$$R(\mathbf{x}_i, \mathbf{x}_j) = \prod_{t=1}^{k} \begin{cases} 1 - 15\left(\theta_t |\mathbf{x}_{i_t} - \mathbf{x}_{j_t}|\right)^2 + .5\left(\theta_t |\mathbf{x}_{i_t} - \mathbf{x}_{j_t}|\right)^3 & 0 \le \theta_t |\mathbf{x}_{i_t} - \mathbf{x}_{j_t}| \le 0.2 \\ 1.25\left(1 - \theta_t |\mathbf{x}_{i_t} - \mathbf{x}_{j_t}|\right)^3 & 0.2 \le \theta_t |\mathbf{x}_{i_t} - \mathbf{x}_{j_t}| \le 1 \\ 0 & \theta_t |\mathbf{x}_{i_t} - \mathbf{x}_{j_t}| \ge 1 \end{cases} \tag{3.14}$$

This two correlation function are compared in figure 3.1. The choice of the

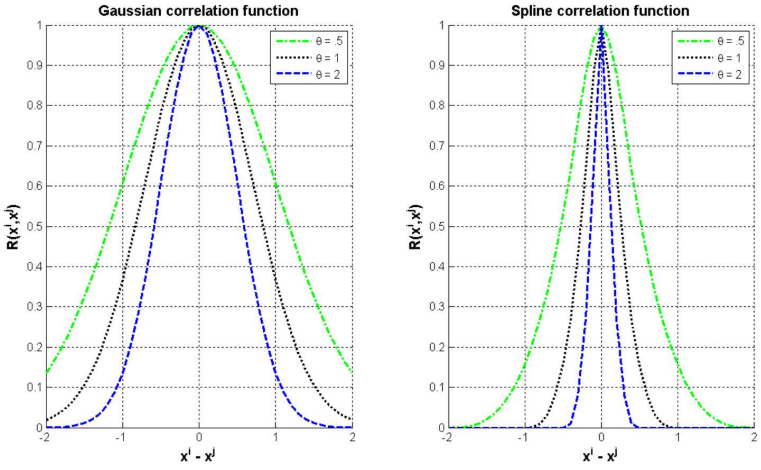

Figure 3.1: Comparison between gaussian and correlation function used in this work

correlation function is rather arbitrary, and among the two most used some authors claim to get better matrix conditioning with the spline function. We didn't experience any matrix conditioning issue when using gaussian correlation function in the work to follow and we also repeatedly compared gaussian with spline function experiencing negligible differences.
No matter what correlation function is used it will always depend on some parameter or set of parameters, that we called θ_t here, that need to be determined before the kriging response can be computed. Values of θ are computed maximizing the *maximum likelihood estimate*, actually minimizing the following functional

$$J(\theta_t) = -\frac{\left[n_s \ln \hat{\sigma}^2 + \ln \|\mathbf{R}(\theta_t)\|\right]}{2} \tag{3.15}$$

[1]Please note that some authors use also

$$R(\mathbf{x}_i, \mathbf{x}_j) = \exp\left[-\sum_{t=1}^{k} \theta_t |\mathbf{x}_{i_t} - \mathbf{x}_{j_t}|^{p_t}\right]$$

leaving p_t to be determined with the maximum likelihood estimation to be described later.

where the variance of the random process $\hat{\sigma}$ is defined as

$$\hat{\sigma} = \frac{\left(\mathbf{y} - \mathbf{f}\hat{\beta}\right)^T \mathbf{R}^{-1} \left(\mathbf{y} - \mathbf{f}\hat{\beta}\right)}{n_s} \tag{3.16}$$

As can be seen by applying proper substitution for $\hat{\beta}$ and $\hat{\sigma}$ in 3.15 the functional is non linear and some kind of global search needs to be emplyed[2].
Once all the θ_k values have been found one can build the kriging response: by switching from polynomial response surface to kriging the user has lost the expression for the response, having gained a nonlinear function modeling capability.
Should the number of training data be too high, either because of a large initial sampling plan or because of an *ad hoc* refinement process, all the matrix operation involved in kriging build up process and model estimation might take a long time to be performed, in that case a multi - CPU parallel approach is necessary. While in the work to follow no parallel approach has been pursued it has been found that when the number of training data is more than a thousand a parallel approach is recommended.

3.3.2 Gradient enhanced kriging

If first derivatives of the true function evaluated at design sites are known it is possible to use this information to build a more accurate response surface. Indeed if higher order derivatives are available one can think of using all this information to augment the kriging. There are basically two ways to accomplish this: the first one, called direct cokriging, exploits gradient information directly, while the second, named indirect cokriging, retains the original kriging formulation on an increased number of sampled data located in the proximity of the original sample point. These added sample points are determined by a Taylor series expansion using gradient information, namely

$$\begin{aligned} x_i^{add} &= x_i + \Delta\mathbf{x}_i \\ y\left(\mathbf{x}_i^{add}\right) &= y\left(\mathbf{x}_i\right) + \Delta\mathbf{x}_i^T \frac{\partial y(\mathbf{x}_i)}{\partial \mathbf{x}} \end{aligned} \tag{3.17}$$

Both methods have been used, the first being more cumbersome in its derivation but probably more accurate, the second being extremely easy to apply but less accurate. Both can be generalized to higher order derivative so that a choice among the two is more a matter of personal taste. In the work to follow we used the direct cokriging approach, and it will be outlined here.
In the original kriging method the covariance matrix of $Z(\mathbf{x})$ in equation 3.7 is equation 3.8. The covariance of the direct cokriging method should be modified to account for gradient information:

$$\begin{aligned} Cov\left(y\left(\mathbf{x}_i\right), y\left(\mathbf{x}_j\right)\right) &= \sigma^2 \mathbf{R}\left[R(\mathbf{x}_i, \mathbf{x}_j)\right] \\ Cov\left(y\left(\mathbf{x}_i\right), \frac{\partial y(\mathbf{x}_j)}{\partial \mathbf{x}_k}\right) &= \sigma^2 \mathbf{R} \frac{\partial R(\mathbf{x}_i, \mathbf{x}_j)}{\partial \mathbf{x}_k} \\ Cov\left(\frac{\partial y(\mathbf{x}_i)}{\partial \mathbf{x}_k}, y\left(\mathbf{x}_j\right)\right) &= -\sigma^2 \mathbf{R} \frac{\partial R(\mathbf{x}_i, \mathbf{x}_j)}{\partial \mathbf{x}_k} \\ Cov\left(\frac{\partial y(\mathbf{x}_i)}{\partial \mathbf{x}_k}, \frac{\partial y(\mathbf{x}_j)}{\partial \mathbf{x}_l}\right) &= -\sigma^2 \frac{\partial R(\mathbf{x}_i, \mathbf{x}_j)}{\partial \mathbf{x}_k \partial \mathbf{x}_l} \end{aligned} \tag{3.18}$$

[2]Usually genetic algorithm or pattern search

so that the covariance matrix of the gradient enhanced kriging looks like

$$\mathbf{R}_c = \begin{bmatrix} Cov\left(y\left(\mathbf{x}_i\right), y\left(\mathbf{x}_j\right)\right) & Cov\left(y\left(\mathbf{x}_i\right), \frac{\partial y(\mathbf{x}_j)}{\partial \mathbf{x}_k}\right) \\ Cov\left(\frac{\partial y(\mathbf{x}_i)}{\partial \mathbf{x}_k}, y\left(\mathbf{x}_j\right)\right) & Cov\left(\frac{\partial y(\mathbf{x}_i)}{\partial \mathbf{x}_k}, \frac{\partial y(\mathbf{x}_j)}{\partial \mathbf{x}_l}\right) \end{bmatrix} \tag{3.19}$$

Kriging prediction equation remains the same in the cokriging too, so that

$$\hat{\mathbf{y}}_c = \hat{\beta}_c + \mathbf{r}_c^T(\mathbf{x})\mathbf{R}_c^{-1}\left(\mathbf{y}_c - \mathbf{f}_c\hat{\beta}_c\right) \tag{3.20}$$

and

$$\hat{\beta}_c = \left(\mathbf{f}_c^T\mathbf{R}_c^{-1}\mathbf{f}_c\right)^{-1}\mathbf{f}_c^T\mathbf{R}_c^{-1}\mathbf{y}_c \tag{3.21}$$

the difference here being that

$$\mathbf{y}_c = \left[\begin{array}{cccccccc} y(\mathbf{x}_1), & y(\mathbf{x}_2), & \ldots, & y(\mathbf{x}_{n_s}), & \frac{\partial y(\mathbf{x}_1)}{\partial \mathbf{x}_1}, & \frac{\partial y(\mathbf{x}_1)}{\partial \mathbf{x}_2}, & \ldots, & \frac{\partial y(\mathbf{x}_{n_s})}{\partial \mathbf{x}_k} \end{array}\right]$$

is the vector of sampled data and associated derivative with respect to each variable,

$$\mathbf{f}_c = \left[\begin{array}{cccccccc} 1, & 1, & \ldots, & 1, & 0, & 0, & \ldots, & 0 \end{array}\right]$$

is a vector of n_s ones and $n_s \times k$ zeros and

$$\mathbf{r}_c^T(\mathbf{x}) = \left[\begin{array}{cccc} R_c(\mathbf{x}, \mathbf{x}_1), & R_c(\mathbf{x}, \mathbf{x}_2), & \ldots, & R_c(\mathbf{x}, \mathbf{x}_{n_s}) \end{array}\right]^T$$

Parameter estimation is performed as in the standard kriging.

3.3.3 Infill strategy

As stated above polynomial response surfaces suffer the lack of an *ad hoc* infill point strategy with which refine the initial sampling plan. One might search the response surface to find its minimum and, after evaluating the true function, add the location of this minimum to the original sampling plan. While this approach might certainly work when considering simple single-minimum function, there is no guarantee that it will converge to the global optimum in case of multi-minima non linear function. Actually this convergence depends heavily on the intial design of experiment. If the DOE puts a design site near the global minimum then there's the chance to find the global minimum by the refinement approach stated above, but if this won't happen the procedure will get stucked in just a local minimum. Using higher order polynomial might work in getting out of local minimum but suffers the already mentioned drawback of unwanted oscillations so that this approach is practically unviable.
One of the main advantage of the kriging method is that, since a gaussian random process has been postulated in its derivation, an equation for uncertainty estimation is available, see e.g. [35, 30],

$$\hat{S}(\mathbf{x}) = \hat{\sigma}\left(\mathbf{f} - \mathbf{r}^T(\mathbf{x})\mathbf{R}^{-1}\mathbf{r}(\mathbf{x}) + \frac{\left(\mathbf{f} - \mathbf{f}\mathbf{R}^{-1}\mathbf{r}(\mathbf{x})\right)^2}{\mathbf{f}^T\mathbf{R}^{-1}\mathbf{f}}\right)^{\frac{1}{2}} \tag{3.22}$$

One possible infill strategy is then to find maximum uncertainty location, evaluate the true function and then augment the initial sampling plan. This approach is extremely useful when the goal is to build up an accurate approximation of

the unknown function and will certainly work in an optimization environment, its convergence to the global minimum will most likely be slow because the infill criteria is minimizing uncertainty and makes non inference on the true function whatsoever.
To accelerate convergence to a global optimum, and keeping in mind the gaussian random process assumption, one can try to find the location where the amount of improvement on the best observed value so far is maximum. In order to do this it's necessary to define the probability of improvement upon the best value so far, namely $I(\mathbf{x}) = y_{min} - y(\mathbf{x})$, y_{min} being the best observed value so far and $y(\mathbf{x})$ being kriging response at location $\mathbf{x}$. The expected *amount* of improvement is then

$$E\left[I(\mathbf{x})\right] = \begin{cases} I(\mathbf{x})\Phi\left(\frac{I(\mathbf{x})}{\hat{\sigma}(\mathbf{x})}\right) + \hat{\sigma}(\mathbf{x})\phi\left(\frac{I(\mathbf{x})}{\hat{\sigma}(\mathbf{x})}\right) & \hat{\sigma}(\mathbf{x}) > 0 \\ 0 & \hat{\sigma}(\mathbf{x}) = 0 \end{cases} \tag{3.23}$$

and we add an infill point to the original sampling plan where equation 3.23 is highest; this location is often searched with a global search method. In equation 3.23 Φ is the cumulative normal distribution function, while ϕ is the normal probability density function.
This is Jone's **E**fficient **G**lobal **O**ptimization algorithm [14], and it is arguably one of the most efficient global optimization methods available[3]; its complete algorithm can be stated as follows:

1. True function evaluation at original sampling plan
2. fit the kriging
3. search for maximum expected improvement location
4. evaluate true function at the above maximum expected improvement location
5. iterate points two, three and four until maximum number of true function evaluations is reached

Following this approach there might be the chance that once the global optimum has been found, the procedure outlined above will add another infill point very close or even at the same location of the optimum just found, resulting in matrix conditioning issue. This situation can be avoided by adding a *distance check* on every new infill point: when the infill point is close to an already sampled location the optimization process is stopped.
On a practical approach, considering the advent of massively parallel computation, one might want to add more infill point at a time. One way would that of using a multiple start procedure with a local optimizer when looking for the maximum expected improvement. Another approach is that of fitting different surrogate and add an infill point where each surrogate suggest it is needed according to a user specified criterion: this might work well as a standalone application or even when using an ensemble of surrogate, see the work of Viana for more details [16, 17, 51].

[3]Many variants of the methods has arisen since then, the most notable being the *Generalized Expected Improvement* and the *Weighted Expected Improvement*. None of them has been used in this work.

Chapter 4

The optimization environment

In this chapter we will describe the tools used in the optimization process and how it was set up. We won't dwell in VLM details, but we'll describe our correction procedure at length, and detail the aerostructural optimization process. Aircraft under optimization will be described first. Flowcharts for our optimization processes can be found in figures 4.1, 4.2 and figure 4.3

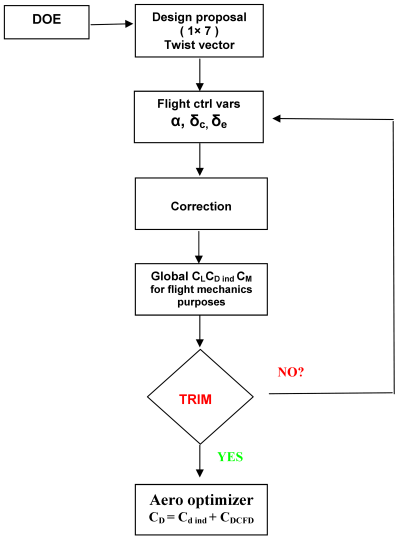

Figure 4.1: Flow chart for twist optimization, rigid aircraft

4.1 The Target Aircraft

The aircraft currently *under optimization* is the **T**arget **A**ircraft, an upscaled variant of the X-DIA model which is a proof-of-concept aeroelastic aircraft

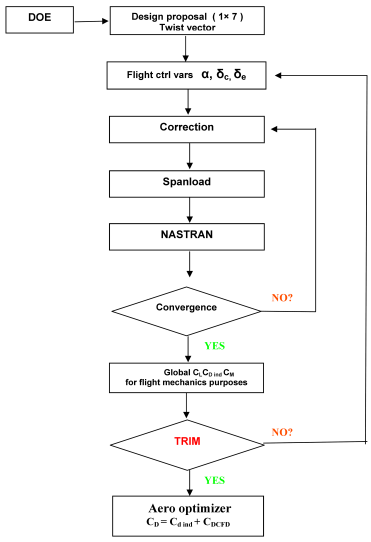

Figure 4.2: Flow chart for twist optimization, elastic aircraft

model used in the framework of the UE-founded 3AS[1] project.
The TA three surface airplane features a 15 degs negative sweep mid-wing with a T tail configuration as can be seen in figure 4.4. Geometrical details can be found in table 4.1.

Scientific debate about the three surface aircraft is endless. Many authors claim for three surfaces superiority, as Kendall in [40, 39, 38], because of the theoretical ability to trim the aircraft with the minimum induced drag possible, no matter where the center of gravity is, provided both the canard and the horizontal tail are independently operated. The situation however is not so clear-cut, drawbacks being additional weight, complexity and interference drag [47], but it is believed that the TA configuration could results in a synergic cooperation between structure and aerodynamic toward weight saving and drag reduction [42].
Cruise conditions for the target aircraft are as in table 4.1

4.2 Twist optimization environment

The design goal of the present work is to develop a geometry with the lowest drag in cruise, which at the same time satisfies lift and pitching moment constraints: to do this we take seven spanwise main wing station of the baseline three surface X-DIA aircraft and use their twist as design variables leaving fixed their geometric properties.

Many other constraints are possible, geometric constraints on the shape of the wing and structural constraints are the most common, but these have not been applied here because of the nature of our design variables. Later we will address root bending and torque moment minimization toghether with drag minimization in a multiobjective environment.

[1]The **Active Aeroelastic Aircraft Structures project**

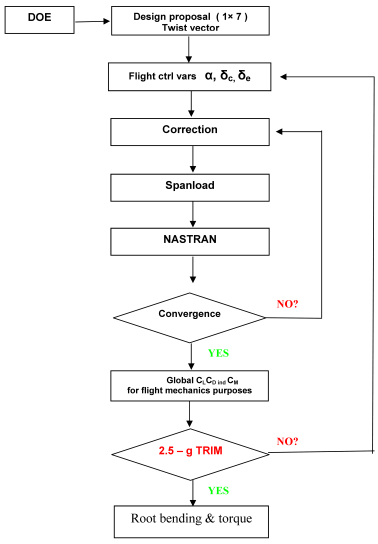

Figure 4.3: Flow chart for twist optimization, elastic aircraft, 2.5 g trim

Based on the above ideas, the mathematical formulation of the optimization problem may be expressed as follows.

$$\begin{gathered} \min C_D \\ w.r.t. \\ C_L = C_{L_{design}} \\ C_{M_{@CG}} = 0 \end{gathered} \tag{4.1}$$

This is not the most common approach to define a wing optimization problem: usually one look for the minimum drag wing that yelds the design lift coefficient with a maximum allowed increase in pithcing moment, so that, see Jameson et al [6], the problem is stated as

$$\begin{gathered} \min C_D \\ w.r.t. \\ C_L = C_{L_{design}} \\ C_M \geq C_{M_{min}} \end{gathered} \tag{4.2}$$

The optimization problem of equation 4.2 is defined this way because usually only the wing is modeled in the computational environment. When, fuselage, engine and tails are modeled their geometry is held fixed during the optimization just to account for aerodynamic effect on the wing under optimization, lift and pitching moment constraints being a way to keep the trim problem into account. On the other hand, optimization problem formulation as in equation 4.1 deals explicitly with the trim problem: our optimum wing is a wing that has the mimimum **trimmed** drag coefficient. This is achieved by modeling the wing, the canard and the horizontal tail and chosing canard, horizontal tail deflections and angle of attack to trim the aircraft everytime a set of aerodynamic design variables is evaluated: basically every time a set of design variables, a twist distribution, is evaluated a trim problem for the three surface aircraft is solved. We believe this is a more realistic and accurate way to optimize the wing,

Symbol	Meaning	Value
$S\ [m^2]$	Wing surface	75
$b\ [m]$	Wing span	30
AR	Wing Aspect Ratio	12
λ	Wing Taper Ratio	0.5
Λ [degs]	Wing Sweep Angle	-15
Root airfoil	NACA	$63_2 - 215$
Tip Airfoil	NACA	$63_2 - 212$
$MAC\ [m]$	Mean Aerodynamic Chord	2.59
$S_C\ [m^2]$	Canard surface	25
$b_C\ [m]$	Canard span	14.14
AR_C	Canard Aspect Ratio	8
λ_C	Canard Taper Ratio	0.5
Λ_C [degs]	Canard Sweep Angle	0
Root airfoil	NACA	$63_2 - 215$
Tip Airfoil	NACA	$63_2 - 215$
$MAC_C\ [m]$	Mean Aerodynamic Chord	1.837
$S_{HT}\ [m^2]$	Tail surface	40
$b_{HT}\ [m]$	Tail span	11.8
AR_{HT}	Tail Aspect Ratio	7
λ_{HT}	Tail Taper Ratio	0.5
Λ_{HT} [degs]	Tail Sweep Angle	20
Root airfoil	NACA	$64 - 009$
Tip Airfoil	NACA	$64 - 009$
$MAC_{HT}\ [m]$	Mean Aerodynamic Chord	1.7519

Table 4.1: TA's geometric properties

Altitude [ft]	26000
Mach number [-]	0.67
MTOW [Kg]	37173.54

Table 4.2: Cruise conditions for the target aircraft

because we are explicitely keeping trim drag into account and that's something that cannot be done formulating the optimization problem as in equation 4.2. Finally, the present approach is similar in principle to that of Ricci et al [42], the difference being that their trim and drag minimization problems are carried out all toghether with the use of an adaptive composite wing and a fixed incidence canard, while we retain a more conventional wing structure, trimming a fixed geometry wing.

4.3 Aeroelastic optimization

As described above the TA is an upscaled version of a proof-of-concept aeroelastic aircraft, so that aeroelasticity need to be taken into account.
When wing flexibility is included, previous chapters' formulation does not change, however things are a little bit diffferent. When performing a rigid wing optimization the analyzed geometry is supposed to be the *1-g* wing, namely the

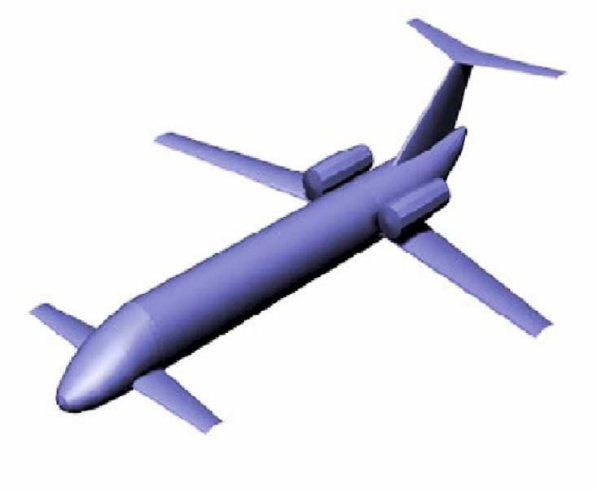

Figure 4.4: Target Aircraft's configuration

optimizer-suggested shape of the wing is thought to be the one under cruise load. On the contrary, when considering an aeroelastic optimization the optimizer-suggested geometry will be the *jig* geometry[2], and the 1-g geometry will come out as part of the solution process, see also [29].
In this work only the wing is considered flexible and its structure is modeled in MSC-NASTRAN with beams elements, while point-mass elements provide inertia loads, and an iterative approach to the aeroelastic problem has been undertaken:

- aerodynamic loads are computated on the supposed rigid surface. As will be explained below, we will just enter our kriging approximation of spanwise lift coefficients and build up spanwise pitching moments coefficients, see section **4.6**
- aerodynamic loads transfer to the FEM model by means of an appropriate interface. Since we have spanwise aerodynamic loads available we just need to interpolate these loads at FEM nodes coordinate, and we do that using a cubic spline. See figure 4.8
- structural deformations computation by means of the finite element model, equation 4.3

  $$\mathbf{Ku} = \mathbf{f} \tag{4.3}$$

  where $\mathbf{K}$ is wing's stiffness matrix, $\mathbf{u}$ nodal displacements' vector and $\mathbf{f}$ is nodal loads' vector, which is the sum of aerodynamic and gravity loads[3]
- structural deformations transfer to the aerodynamic mesh with an appropriate interface. Having nodal rotations we, again, interpolate them with a cubic spline to find the new wing twist, see figure 4.9. This effective twist

[2]Provided gravity forces are taken into account, see [45]
[3]Actually we could have approximated NASTRAN behaviour with a kriging with a linear mean model, but we decided to leave it at that

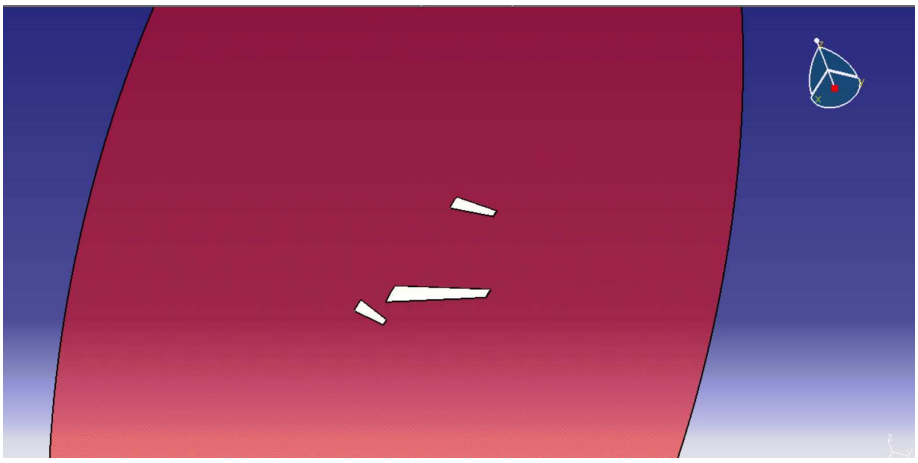

Figure 4.5: CATIA CFD model of the Target Aircraft. Note in red the simmetry plane

distribution is used as a new boundary condition for a new aerodynamic solution

- Iterate until convergence

We deem the aerostructural loop to be converged when the difference between current and previous tip rotation is less than a specified tolerance. This tolerance was set on the basis of a sensitivity of global aerodynamic coefficients to local twist, so that to perform a jig - 1g loop usually 8, and no more than 10 iterations were needed.

4.4 Three surface aircraft trim

As stated abover we're dealing with a three surface aircraft and we decided to operate the canard and the horizontal tail independently to achieve a trimmed condition.
The basic idea behind the three surface aircraft is that by having a lifting surface ahead of the main wing aircraft's induced drag should be less, however, as seen on the Piaggio P-180 and on the baseline X-DIA aircraft, canard is usually fixed, its deflection being decided during design, and is not used for trim. On the contrary, we reasoned that to fully exploit three surfacce aircraft advantage canard deflection too should be used to trim the aircraft, and it should be operated indipendently of the horizontal tail [40, 39, 38]. While this might be an unconvential design solution it is not different in principle to what is already implemented on most modern commercial aircraft for the horizontal tail. Basically the horizontal tail is split in two different part, the horizontal stabilizer and the elevator, but for trim purposes the entire horizontal surface is used as a control. We are assuming we can do the same on the canard too without incurring in an excessive weight penalty.
This choice adds some complexity to the problem as is going to be described

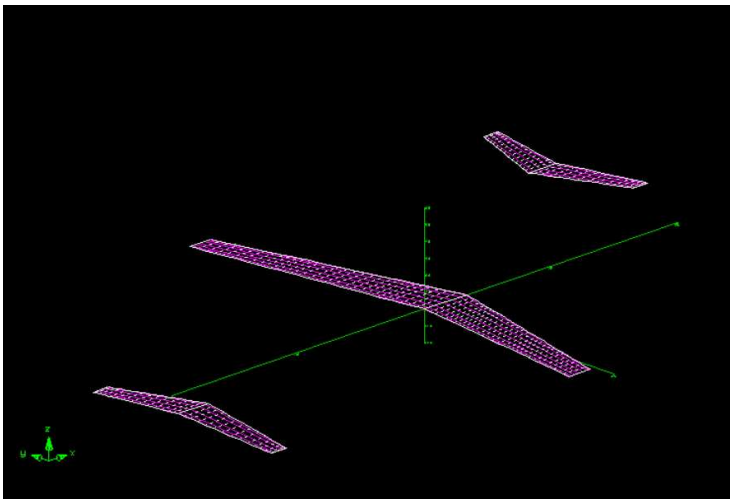

Figure 4.6: AVL vortex lattice model of the Target Aircraft

below.
For a two surface aircraft the trim problem is stated as

$$\begin{aligned} C_L &= C_{L_0} + C_{L_\alpha}\alpha + C_{L_\delta}\delta = \frac{n_z W}{q_\infty S} \\ C_{M_{@CG}} &= C_{M_0} + C_{M_\alpha}\alpha + C_{M_\delta}\delta = 0 \end{aligned} \tag{4.4}$$

In equation 4.4 α is aircraft angle of attack, δ is horizontal tail deflection, C_{L_α}, C_{L_δ}, C_{M_α}, C_{M_δ} are well known flight mechanics aerodynamic derivative, n_z is aircraft load factor, W is aircraft's weight, q_∞ is dynamic pressure and S is aircraft's reference surface. In the incompressible regime this is an algebraic linear system of equation, while in the transonic regime this is a non linear system. Disregarding linearity, the main point here is that for a two surface aircraft, such as the one descirbed by equation 4.4, there are two equations and two unknowns so that the system is closed and the solution unique no matter what the employed aerodynamic model is.
For a three surface aircraft there will be three unknowns with two equations

$$\begin{aligned} C_L &= C_{L_0} + C_{L_\alpha}\alpha + C_{L_{\delta_c}}\delta_c + C_{L_{\delta_e}}\delta_e = \frac{n_z W}{q_\infty S} \\ C_{M_{@CG}} &= C_{M_0} + C_{M_\alpha}\alpha + C_{M_{\delta_c}}\delta_c + C_{M_{\delta_e}}\delta_e = 0 \end{aligned} \tag{4.5}$$

In equation 4.5 δ_c is canard deflection and δ_e is horizontal tail deflection. To close the system and trim the aircraft one has to add a condition like the minimization of the trim drag so that the **close** three surface aircraft trim problem is

$$\begin{aligned} &\min C_D \\ &w.r.t. \\ &C_L = \frac{n_z W}{q_\infty S} \\ &C_{M_{@CG}} = 0 \end{aligned} \tag{4.6}$$

This is an optimization problem in three variables, namely angle of attack, canard and horizontal tail deflections, and many different approach were considered here, including simple kriging, gradient enhanced kriging and gradient

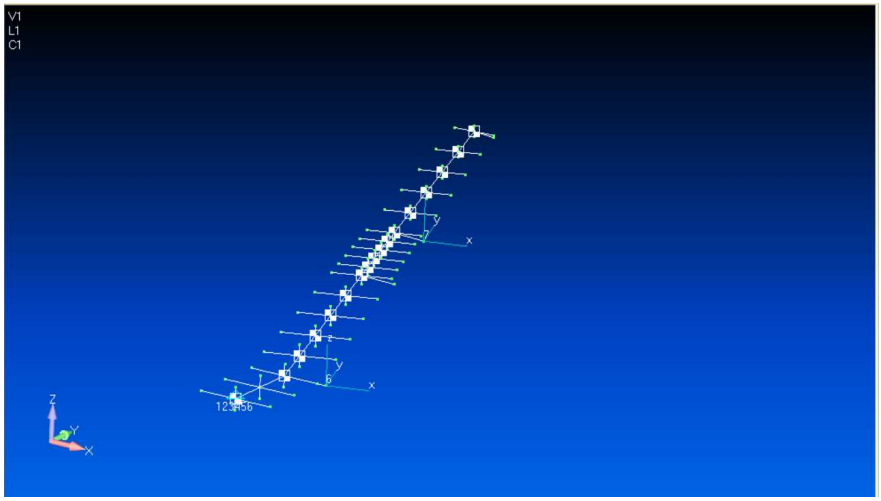

Figure 4.7: MSC/NASTRAN employed stick model for aeroelastic computations

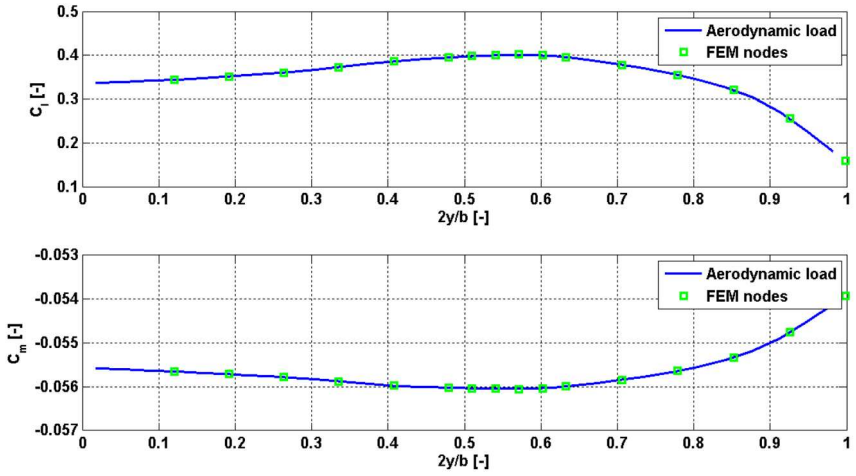

Figure 4.8: Load transfer between the aerodynamic model and the FEM

based optimization methods[4]. While they all succeeded[5] the direct gradient based method has been preferred because of a more simple and immediate implementation; a multiple restart approach shown a less-than-a-count sensitivity to the initial guess suggesting a reasonably flat design space.

[4]Global search has been considered too but they would have let the CPU time of the overall aerodynamic optimization suite grows too high. Beside, as explained later, it turned out that they were not needed

[5]When using any of the two kriging methods above lift and pitch constraints were applied with the penalty function method and we found that the following objective function was well suited to trim the aircraft

$$F = C_D + 100\left(C_L - C_{L_{design}}\right)^2 + 50\,(C_M)^2$$

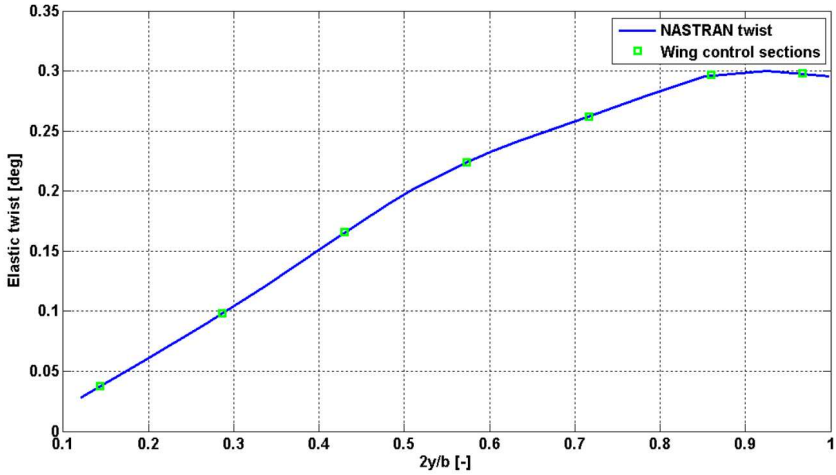

Figure 4.9: Twist transfer between the FEM and the aerodynamic model

4.5 Transonic vortex lattice correction

The vortex lattice method is a well known aerodynamic tool that provide accurate and useful result in the incompressible regime at a very limited CPU cost, whose details can be found in [25, 26] and will not be dealt with here.
VLM methods rely on linear aerodynamic theory so that they cannot be used in the transonic regime. Their generalization in the compressible low Mach regime is achieved with Prandtl Glauert or similar theory, yielding good results because the flow is shock free. These corrections cannot however be trusted in an optimization environment, for their assumption will certainly be heavily violated because of exploration of an unfavourable non-shock-free zone of the design space. Considering transonic aerodynamic optimization this means that even though the optimum will be a shock free solution, for which Prandtl Glauert theory can give good result, the optimizer will need to evaluate possible non-shock-free design, and in this case Prandtl Glauert correction cannot be trusted upon, feeding the optimization algorithm with inaccurate information. This is even more true considering the global search nature of the EGO algorithm used here.
To circumvent this problem, while retaining upon a simple geometry description needed in early design phases, we apply a correction procedure to the VLM method based upon two dimensional quick-to-evaluate CFD results. We will basically require local lift coefficient from the VLM to be equal to 2D transonic CFD data once local induced angle of attack has been take into account. This idea is not a novel approach, previous studies can be found in [44, 37, 19, 20, 10, 36, 46], but we believe it is innovative in the way it is achieved.
As an off-line phase of the correction process two dimensional transonic airfoil polars[6] has been computed for each of the seven spanwise station with the EDGE flow solver, see figure 4.10. We used a structured O-grid, figure 4.11, with low

[6]Pitching moment coefficient computed at chord's quarter point

Reynolds number resolution and the Spalart Allmaras turbulence model, judging convergence with a order-of-magnitude residual drop criteria, force convergence and eddy viscosity, figures 4.12 and 4.13.

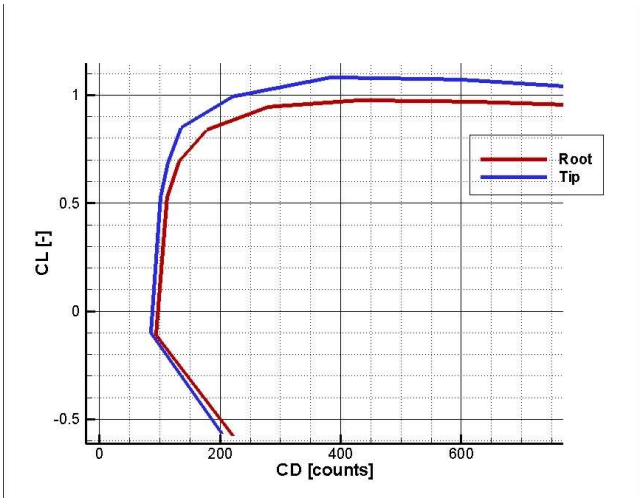

Figure 4.10: Two dimensional root and tip airfoils polars

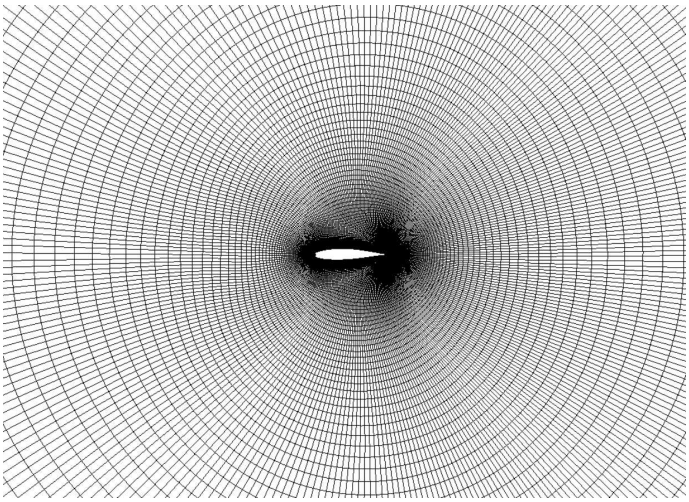

Figure 4.11: Two dimensional high quality structured mesh used for airfoil polars computations

Airfoil polars were computed at reference freestream Mach number $M = 0.65$, the one that stem from simple sweep theory applied to the main wing, namely

$$M_{sweep} = M_{\infty} \cos(\Lambda) \tag{4.7}$$

and M_{∞} is the **TA** cruise mach number, see table 4.1. With these CFD data we can start the correction process. We ask AVL local lift coefficient at those spanwise station mentioned above to be equal to CFD lift coefficient taking into

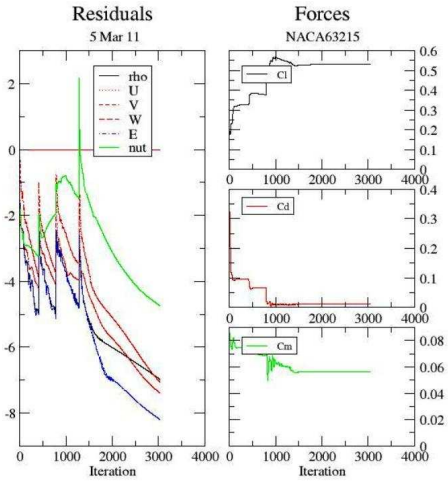

Figure 4.12: Typical convergence history for two and three dimensional computations

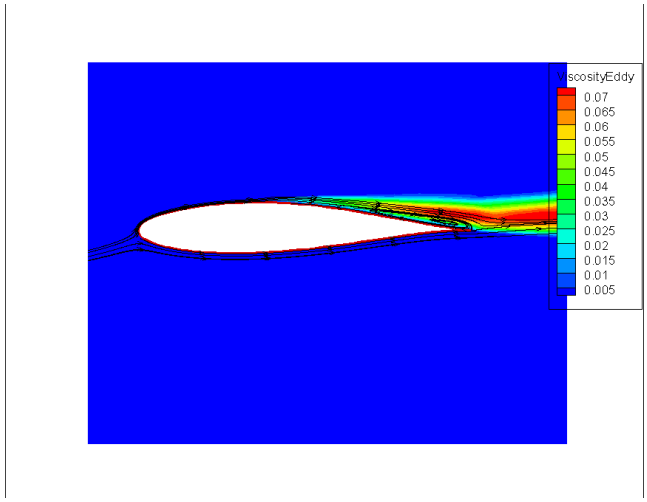

Figure 4.13: Eddy viscosity contours for the root airfoil at $\alpha = 6$ deg

account the induced angle of attack computed with AVL. Since in general this will not be true, we'll iterate until this condition is satisfied adding an extra, fictitious twist to the original one as explained below. There are many ways to do this, we found the most efficient is to state the problem as an optimization problem. Writing the cost function as

$$F\left(\mathbf{TWIST_2}\right) = \sum_{i=1}^{7} \left(C_{L_{AVL_i}}\left(\alpha_{1_i}\right) - C_{L_{CFD_i}}\left(\alpha_{2_i}\right)\right)^2 \tag{4.8}$$

we state that

$$\begin{aligned} \alpha_{1_i} &= AOA + \alpha_{ind_i} + TWIST_{1_i} + TWIST_{2_i} \quad i = 1 \ldots 7 \\ \alpha_{2_i} &= AOA + \alpha_{ind_i} + TWIST_{1_i} \quad i = 1 \ldots 7 \end{aligned} \tag{4.9}$$

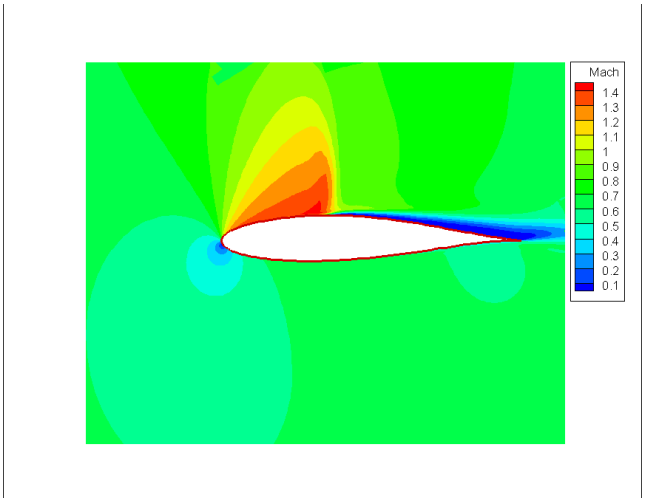

Figure 4.14: Mach contours for the root airfoil at $\alpha = 6$ deg

being $\mathbf{TWIST_{2_i}}$ the fictitious twist value necessary to achieve the minimum of the functional in equation 4.8, i.e. the optimization variables, and AOA being the overall aircraft's angle of attack.
Basically what is happening here is this: first the aerodynamic twist optimization algorithm will give a candidate $\mathbf{TWIST_1}$ (1×7) vector of wing twist section, second we set up the optimization problem in 4.8 using the vector $\mathbf{TWIST_2}$ as the optimization variable. Once this optimization problem has been solved we proceed to evaluate the aerodynamic twist-optimization cost function.
Equation 4.8 can be minimized using any optimization algorithm available, but thinking of it as a non linear least square problem helps in reducing the overall number of function evaluation required since common gradient based non linear least square techniques, we used the powerful MatLab `lsqnonlin`, can be used. Optimization initial guess was not an issue because of low values' cost function achieved[7]. There remain one question open, namely where to apply optimization problem 4.8 in the overall twist optimization process, and possible answers are as follows:

- on line, during twist optimization iteration and keeping AVL in the loop
- on line, during twist optimization iteration, AVL out of the loop and output from AVL being approximated by a surrogate
- off line, building surrogates of any element of $\mathbf{TWIST_2}$ vector that satisfy equation 4.8.

The first option is unfeasible because it would rise the CPU time too much, violating our primary goal. Second option might succeed, while the third one is the one that we actually used.

[7] Usual cost function was

$$F = 1e - 9$$

and change in initial guess resulted only in one order of magnitude variations at most

Keeping AVL in the loop is simply too expensive and we do not actually need it because of the aformentioned linearity of vortex lattice method. Main VLM assumption is linearity so that VLM results are linear too, and this holds true for spanwise lift coefficient and angle of attack, as can be seen in figures 4.17 and 4.18 for a two variable twist vector case.

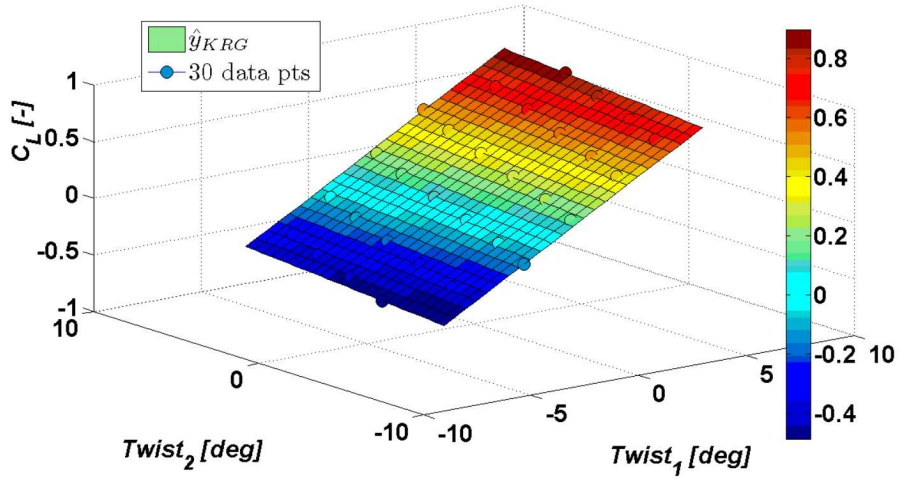

Figure 4.15: Local lift coefficient linearity for a two variables case

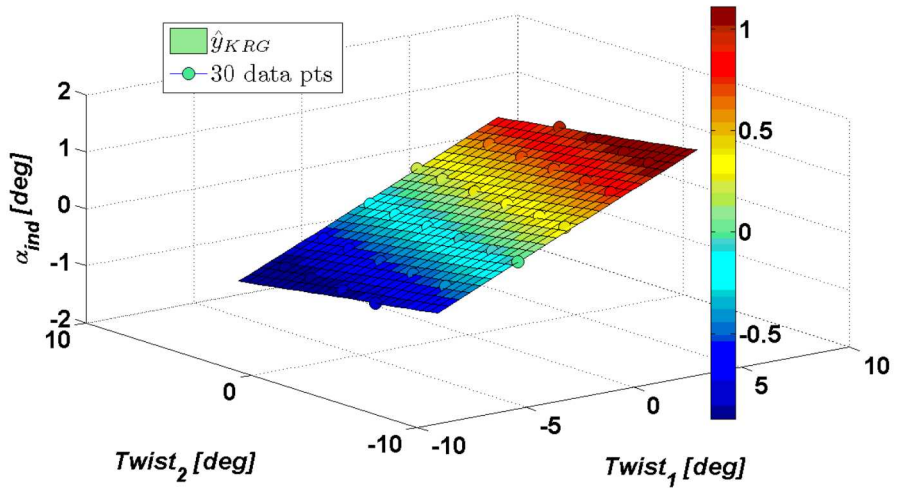

Figure 4.16: Local induced angle of attack linearity for a two variables case

Because of this, there's no real reason to keep AVL in the loop, there's only the need to build up a surrogate of **each** spanwise lift coefficient and induced angle of attack, and this can be done with a limited number of AVL calls. For this purpose we actually used a latin hypercube sampling made up of 450 design sites. However, note that local lift coefficient and induced angle of attack depend on wing twist, aircraft angle of attack, canard and horizontal tail deflections, so

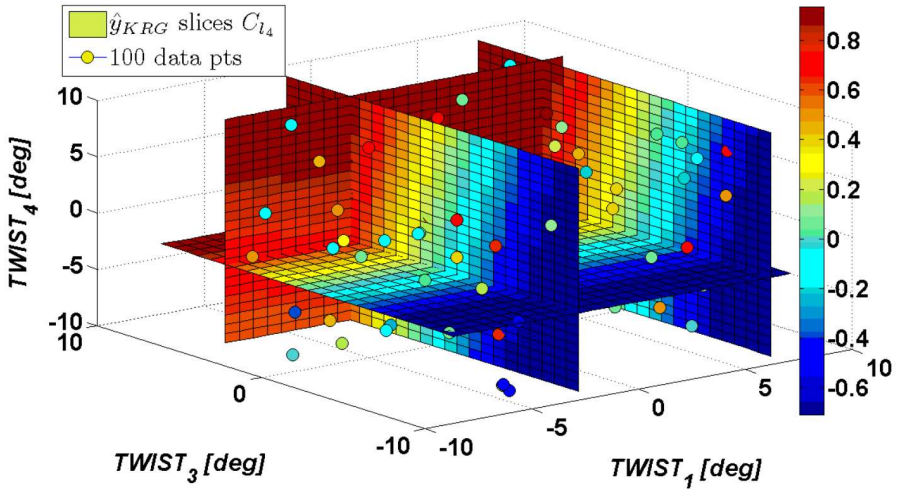

Figure 4.17: Local lift coefficient for the fourth twist section. Slices from the ten dimensional design space

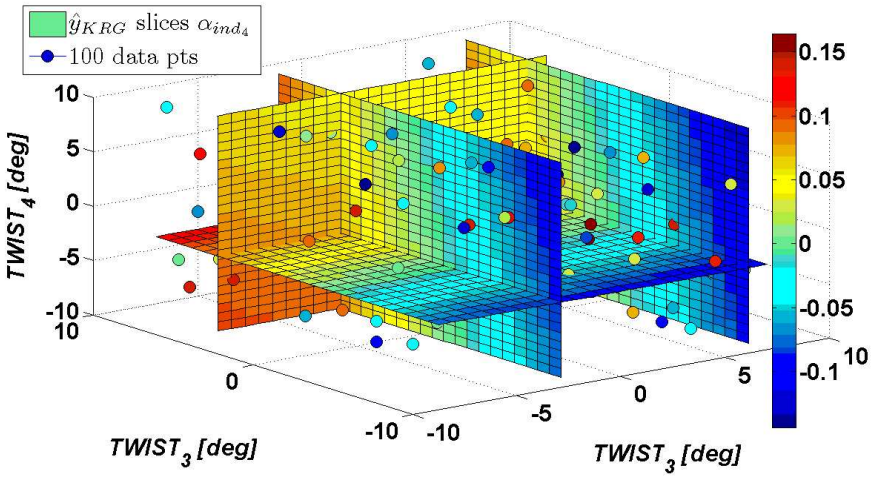

Figure 4.18: Local induced angle of attack for the fourth twist section. Slices from the ten dimensional design space. Contours are in radians

that each surrogate is a ten variables surrogate.
What we need are local lift coefficient and induced angle of attack at those seven spanwise station used in the aerodynamic twist optimization in order to match CFD and VLM results. We could have kept AVL in the optimization process 4.8 but it turned out it was extremely computational expensive. Exploiting the full advantage of AVL's linearity we decided to mimick AVL-needed data using some sort of surrogate, all we need is to know what variables affects local lift and induced incidence. Evidently we can write equations 4.10 and 4.11

$$C_{L_i} = C_{L_i}\left(AOA, \delta_c, \delta_e, \mathbf{TWIST}\right) \;\; i = 1 \ldots 7 \tag{4.10}$$

$$\alpha_{ind_i} = \alpha_{ind_i}\left(AOA, \delta_c, \delta_e, \mathbf{TWIST}\right) \;\; i = 1 \ldots 7 \tag{4.11}$$

and here **TWIST** is the sum of both $\mathbf{TWIST_1}$ and $\mathbf{TWIST_2}$. Since **TWIST** is a (1×7) vector, local induced angle and lift coefficients depend upon a total of ten variables.
However it turns out that AVL local coefficients are noisy[8] so that among all the surrogate we decided to use polynomial response surface of order one[9].
Having taken the use of metamodeling this far we subsequently decided to build surrogates also of AVL global lift, induced drag coefficients, canard and horizontal tail lift and pitching moment too. Again we can write

$$\begin{aligned} C_L &= C_L\left(AOA, \delta_c, \delta_e, \mathbf{TWIST}\right) \\ C_{D_{ind}} &= C_{D_{ind}}\left(AOA, \delta_c, \delta_e, \mathbf{TWIST}\right) \\ C_{L_{canard/Htail}} &= C_{L_{canard/Htail}}\left(AOA, \delta_c, \delta_e, \mathbf{TWIST}\right) \\ C_{M_{canard/Htail}} &= C_{M_{canard/Htail}}\left(AOA, \delta_c, \delta_e, \mathbf{TWIST}\right) \end{aligned} \tag{4.12}$$

so that with a total of 450 AVL evaluations we mimicked AVL **throughout** the activity; for all lift and pitching moment coefficients we retained a PRS of order one while for the induced drag we, obviously, used a PRS of order two[10].
Now we don't need AVL anymore when minimizing equation 4.8: for a given set of flight control variables and $\mathbf{TWIST_1}$ vector the non linear least square technique used gives a $\mathbf{TWIST_2}$ vector guess. With each element of it we enter the response surface approximation of equation 4.11, so that we can evaluate equation 4.9, and the approximation of equation 4.10. Upon entering each 2D CFD airfoil polar with each $\boldsymbol{\alpha_2}$ vector's element we get $C_{L_{CFD_i}} \;\; i = 1 \ldots 7$ in equation 4.8 and we can proceed to minimization.
Once equation 4.8 has been minimized we have a relation of the form

$$\mathbf{TWIST_2} = f\left(AOA, \delta_c, \delta_e, \mathbf{TWIST_1}\right) \tag{4.13}$$

and that's all we need to apply the correction. Now we have to choose either to keep optimization problem 4.8 in the twist-optimization loop, or to build up a surrogate of equation 4.13, actually one surrogate each element of the $\mathbf{TWIST_2}$ vector. To take a decision we reasoned that equation 4.8 should be linear up to CFD stall angle, deviating from linearity there on: this behaviour can be easily approximated by the kriging, see figure 4.19 for a two dimensional test case. Glancing at equation 4.13 we see that the $\mathbf{TWIST_2}$ vector is, again, a function of ten variables therefore we built a (1750×10) latin hypercube design, run the non linear least square problem and then fit the kriging: time to fit was significant, but we managed to fit all seven kriging in approximately an hour.
Now the correction process is completed: as the twist optimization algorithm gives the twist distribution, vector $\mathbf{TWIST_1}$ in equation 4.9, and the trim suite gives a set of flight control we can enter twist correction kriging and get the necessary $\mathbf{TWIST_2}$ vector to satisfy equation 4.8.
We decided to apply the described correction procedure to the main wing only fot the sake of simplicity, we do not believe that this will be a major source

[8] An undesirable feature shared by any vortex lattice method

[9] Results from a regressing kriging gave the same result as well but we opted for PRS because of the slight speed improvement in computing the response

[10] It turned out that global coefficients are much less noisy than local ones

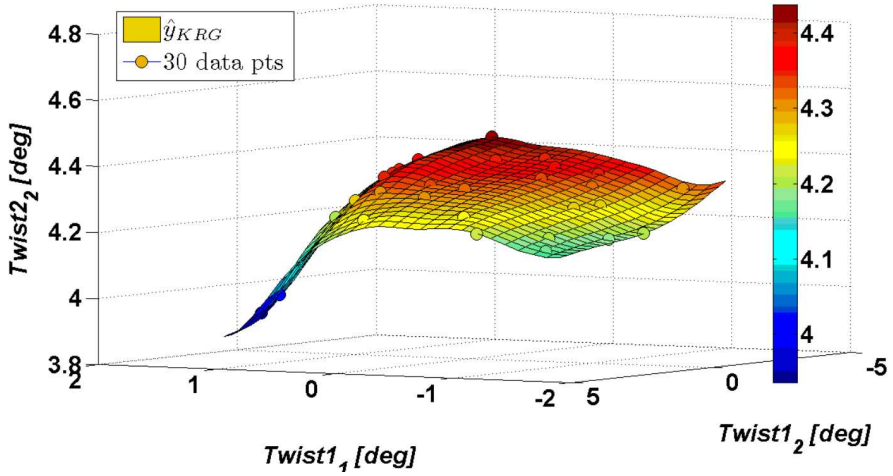

Figure 4.19: Kriging approximation of the second element of the $\mathbf{TWIST_2}$ vector in equation 4.13 for a two dimensional test case.

of error for at high speed control surfaces deflections should be small and no shock is expected on control surfaces: in this situation simple Prandtl Glauert correction suffice.

4.6 Coefficients buildup

Once the $\mathbf{TWIST_2}$ vector has been determined from the kriging using the design twist vector $\mathbf{TWIST_1}$ and the set $(AOA, \delta_c, \delta_e)$ we can compute all aerodynamic coefficients needed. Aircraft overall lift, which is the first of the two constraints in equation 4.6, induced drag and control surfaces' pitching moment coefficients come from surrogate approximation of equation 4.12; we're left with main wing coefficients computation. With the second of equation 4.9 we enter two dimensional airfoils polar to get local lift[11], drag and moment coefficients: upon spanwise integration of local drag coefficients, equation 4.14,

$$C_{D_{CFD}} = 2\int_0^{b/2} c(y) C_{D_{2D}}\, dy \tag{4.14}$$

we get main wing viscous and shock drag coefficients, $c(y)$ being main wing chord distribution. Overall aircraft drag coefficient, neglecting control surfaces' pressure and viscous drag, is

$$C_D = C_{D_{IND}} + C_{D_{CFD}} \tag{4.15}$$

Equation 4.15 is the cost function of the aerodynamic optimization problem 4.1. Wing pitching moment coefficient is computed in the same fashion, equation

[11] To be precise two dimensional lift coefficient can either be taken from two dimensional CFD data or from AVL kriging approximation of equation 4.10 because we have satisfied equation 4.8

4.16,

$$C_{M_{wing}} = 2\int_0^{b/2} c(y)\left(C_{M_{CFD}} + e(y)C_{L_{2D}}\right) dy \tag{4.16}$$

$e(y)$ being distance between local quarter chord and center of gravity location[12]. Once $C_{M_{wing}}$ has been computed the overall aircraft pitching moment is

$$C_{M_{@CG}} = C_{M_{wing}} + C_{M_{canard}} + C_{M_{HTail}} \tag{4.17}$$

which is the last of the two constraints in the trim optimization problem 4.6. When dealing with an aerostructural case we also use local lift and pitching moment coefficients to load the finite element model. In this cases local lift is defined as in equation 4.18

$$l(y) = q_\infty c(y) C_{L_{2D}} \tag{4.18}$$

where $q_\infty = \frac{\gamma}{2} p_\infty M_\infty^2$ is the freestream dynamic pressure; quite the same way local torque moment is as in equation 4.19

$$m_y(y) = q_\infty c(y)\left(C_{M_{2D}} + d(y)C_{L_{2D}}\right) \tag{4.19}$$

$e(y)$ being distance between local quarter chord and elastic axes.

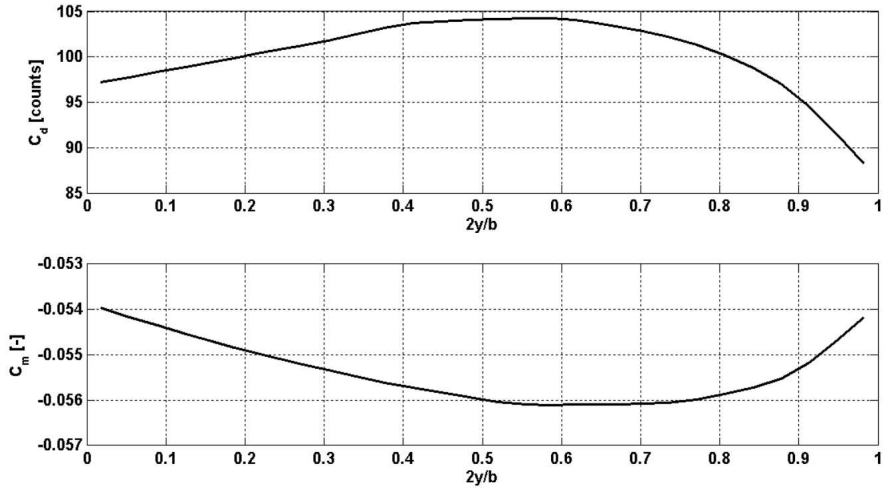

Figure 4.20: Drag and moment coefficients build up

[12] Actually we should be using C_Z instead of C_L but we're under small angles assumption

Chapter 5

Optimization results

Having described the optimization suite we built up in the previous chapter, we're now going to see some of the achieved results. We will start with an isolated wing test case, then switch to the the full **TA** aircraft. Design variables are twists of those seven spanwise station discussed above. They will **all** be left free to vary between a minimum of -5 degrees and a maximum of 5 degrees[1], see table 5.1. For both the isolated wing and the whole aircraft results will be compared against EDGE three dimensional computations with the Spalart-Allmaras turbulence model and a $y^+ = 1$ boundary layer resolution[2]. CATIA CAD models, e.g. figure 4.5, have been paramterized in all the relevant varibles, meaning seven spanwise sections' twist and canard and horizontal tail deflections. Main wing's airfoil, see table 4.1, have been defined with the use of CST parameterization [41, 7].
In order to perform meaningful comparisons between optimized and baseline three dimensional geometries all computational **unstructured**[3] meshes have been generated with the same settings through the use of appropriate scripts: in building the meshes, see for examples figure 5.1, we followed guidelines' from the third AIAA Drag Prediction Workshop [12] as far as possible according to the limited computational resources available.

	Minimum	Maximum
Twist [deg]	-5	5
AOA [deg]	0	3
δ [deg]	-5	5

Table 5.1: Bounds for both the aerodynamics and the twist optimization throughout the work

[1] Different twist parameterizations have been considered too, one that allowed a maximum twist increment between two consecutive section have actually been employed but no significant advantage could be gained from its use

[2] Geometrical first cell height has been taken from two dimensional data

[3] Boundary layer has been resolved with anisotropic tetrahedral elements

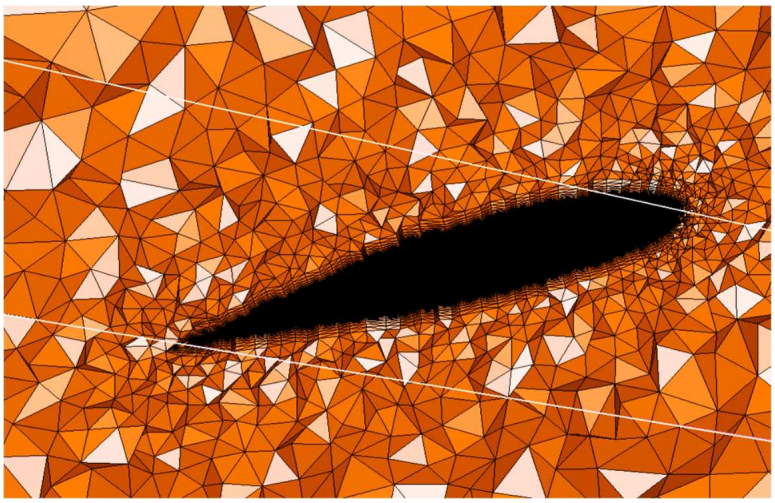

Figure 5.1: Close up view unstructured mesh. Note anisotropic tetrahedral element to accurately resolve the boundary layer

5.1 Isolated wing test case

As the first application of the optimization environment described in the previous chapter we decided to consider a simple isolated wing test case. The wing is the same negative sweep X-DIA aircraft wing, see figure 5.3, but no control surfaces are present in the model. We performed a constrained optimization of this wing both in the incompressible regime, where AVL results were not corrected, and in the transonic regime, where we used our correction procedure; lift and pitching moment constraints can be found in table 5.2.
Results achieved in this section will give us a feeling of a negative sweep wing behaviour and data to judge full aircraft optimization results.

	Value
$C_{L_{target}}$	0.35
$C_{M_{target}}$	-0.38

Table 5.2: Lift and pitching moment constraints for the isolated wing optimization's test case. These values has been chosen because they're representative of main wing's Target Aircraft loads

5.1.1 Incompressible isolated wing test case

Here we present incompressible vortex lattice optimization of the **TA** main wing. Being in the incompressible regime means that AVL results can be trusted and no correction need to be applied. We will first optimize induced drag under a lift constraint, then we will add a pitching moment constraint as in equation 4.2. To the seven design variables discussed above we also let the angle of attack free to vary. As an optimization algorithm we used a kriging with a second order polynomial mean model and gaussian correlation function. The original DOE

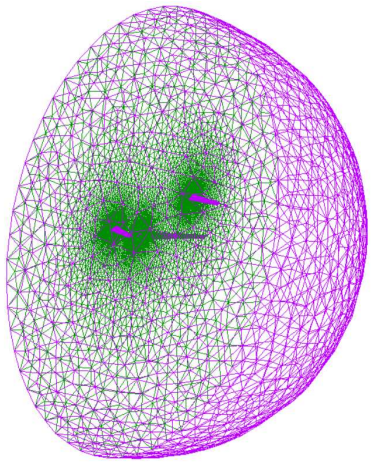

Figure 5.2: Far field view of the unstructured three dimensional mesh

has been refined with the EGO approach.
For the lift constrained optimization we used the cost function described in 5.1

$$F = C_D + 100\left(C_L - C_{L_{target}}\right)^2 \tag{5.1}$$

Lift constraint has been satisfied, no bound has been reached or violated and the optimum induced drag coefficient is

$$C_D = 32\ counts$$

and spanwise load distribution can be seen in figure 5.4 This is no surprise, we achieved a nearly elliptical lift distribution in good agreement with Prandtl lifting line theory. Close to the root lift start to decrease because root airfoil is not allowed to twist, this should help simulating fuselage effects.
Just for comparison purpose it is important to note that this wing pitching moment coefficient, referred to the same location as the center of gravity would be found for the whole aircraft, is

$$C_{M_{@CG}} = -0.4025$$

When including a pitching moment constraint things get a little bit different. We applied the same optimization procedure as for the lift constrained wing, just changing the cost function to equation 5.2

$$F = C_D + 100\left(C_L - C_{L_{design}}\right)^2 + 50\left(C_M - C_{M_{target}}\right)^2 \tag{5.2}$$

Spanwise load distribution for this optimization can be seen in figure 5.5

Both constraints are satisfied, no bounds has been reached or violated while the induced drag coefficients is

$$C_D = 47\ counts$$

With the added constraint we lost 15 counts and the nearly elliptical lift distribution. This is an important result to keep in mind for a very similar lift

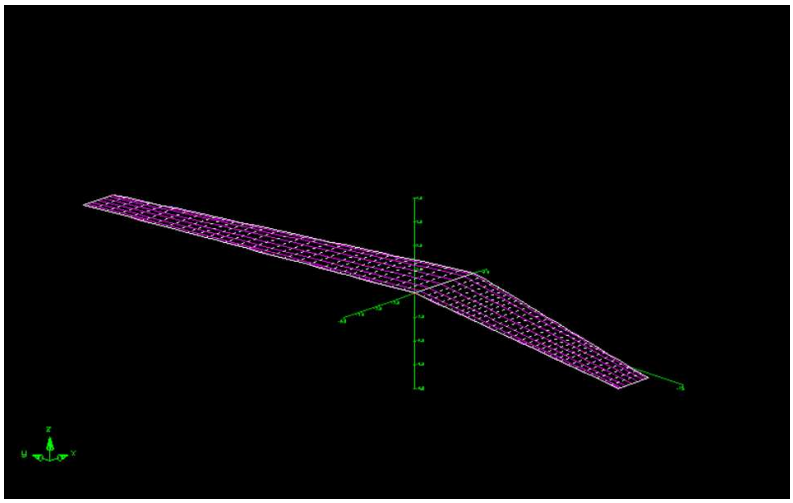

Figure 5.3: AVL isolated wing model

distribution will be seen when considering full aircraft results. This is a consequence of the negative sweep wing: most inboard airfoils are far away from pitching moment reference point so that they can have less lift with respect to tip airfoil which are quite close to the moment reference point and need to produce much more lift in order to satisfy the pitching moment constraint. This is an extremely undesirable feature from an airworthiness point of view for the most outer part of the wing will stall first, but more about this will be said later.

5.1.2 Transonic isolated wing test case

Here we're going to analyze results from a transonic wing optimization. The main difference from the previos section is the presence of our correction process discussed in the previous chapter. We have chosen the same cruise condition as that of the Target Aircraft, see table 4.1, and while relying upon the same cost function as in equation 5.1, we have here

$$C_D = C_{D_{IND}} + C_{D_{CFD}} \tag{5.3}$$

the same as in the full aircraft optimization, equation 4.15. Lift constraint is satisfied, no bound has been reached or violated and the **corrected** drag coefficient is

$$C_D = 134 \; counts$$

and for the purpose of comparison wing pitching moment is

$$C_{M_{@CG}} = -0.4876$$

Spanwise lift distribution can be seen in figure 5.6, and once more a nearly elliptical lift distribution has been achieved. We decided to evaluate baseline wing's performance for the purpose of comparison with the optimized wing. Results are reported in table 5.3: since wing's angle of attack has been used as a variable during the optimization, we run the baseline wing at the appropriate angle

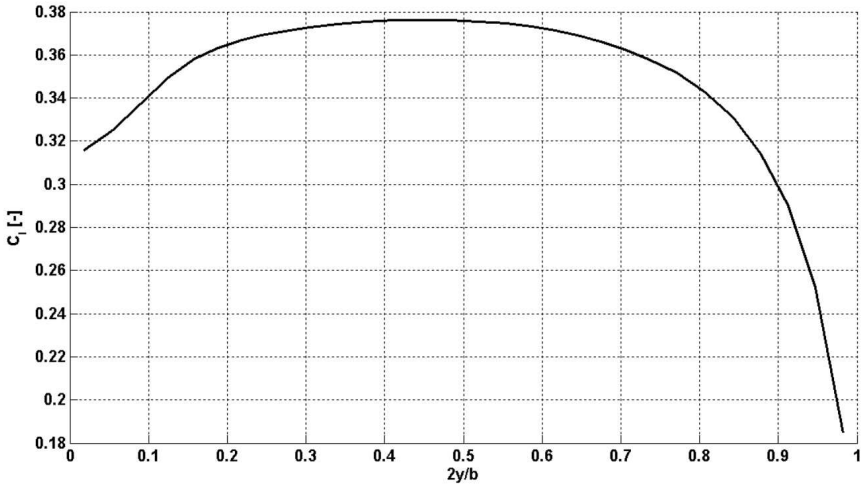

Figure 5.4: Optimized incompressible spanwise lift distribution. Lift-constrained isolated wing test case

of attack to achieve the target lift coefficient, finding out that we just gained 3 *counts* in the optimization. Lift distribution comparison between the baseline and optimized wing can be found in figure 5.7.

	C_D	C_L	C_M
Baseline	137	0.35	-0.5044
Optimized	134	0.35	-0.4876

Table 5.3: Comparison between baseline and optimized wing

Applying a pitching moment constraint changes lift distribution in figure 5.6 considerably, exactly as in the incompressible case. We use the same cost function as in equation 5.2 with the drag coefficient defined as in equation 5.3. Both constraints are satisfied, no bound has been reached or violated but this time the drag coefficient is

$$C_D = 156 \; counts$$

Spanwise lift distribution can be seen in figure 5.8 where once again we can see how the most outer part of the wing is loaded and how lift distribution changes in the transonic regime because of our correction process.

Having achieved results for the isolated wing test case it's appropriate that we proceed to a comparison with three dimensional CFD results. CFD computation for the lift constrained wing at the same angle of attack as predicted by our optimization process shows that our optimizer has driven us towards a shock-free wing[4]. Overall lift, drag and pitching moment coefficients can be seen in table 5.4. These are very good results, especially considering the very

[4]As Jameson pointed out in [32] the attainment of a shock-free flow is a demonstration of a successful drag minimization

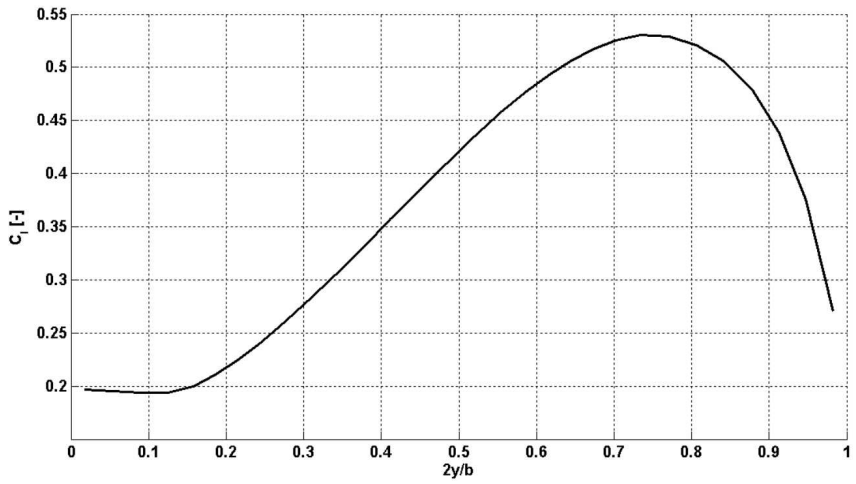

Figure 5.5: Optimized incompressible spanwise lift distribution. Lift and pitch-constrained isolated wing test case

high level of approximation involved in our optimization process, even though coefficients are a little bit overpredicted. In order to understand if we can rely on our optimization procedure, both in a preliminary design environment and in a more advanced design phase using it as a low fidelity model, we need to compare optimized wing's EDGE results with those from the baseline, aiming to understand if our optimization process is able to capture coefficients variations accurately, and this can be seen in table 5.5. It can clearly be seen that the optimized wing has effectively less drag than the baseline wing. Coefficients are overpredicted by EDGE for both the baseline and optimized wing, but it would look like increments are predicted correctly.

	C_D	C_L	C_M
AVL corrected	134	0.35	-0.4876
EDGE	163	0.3639	-0.4634

Table 5.4: Comparison between AVL optimized wing and EDGE evaluation of the optimized geometry at the same angle of attack predicted by AVL.

	$C_{L_{target}}$	C_L	C_D	C_M
BASELINE	0.35	0.3668 (0.35)	168 (137)	-0.4845 (-0.5046)
Optimized	0.35	0.3639 (0.35)	163 (134)	-0.4634 (-0.4876)

Table 5.5: EDGE comparison between optimized and baseline wings, AVL corrected results in parenthesis for ease of comparison

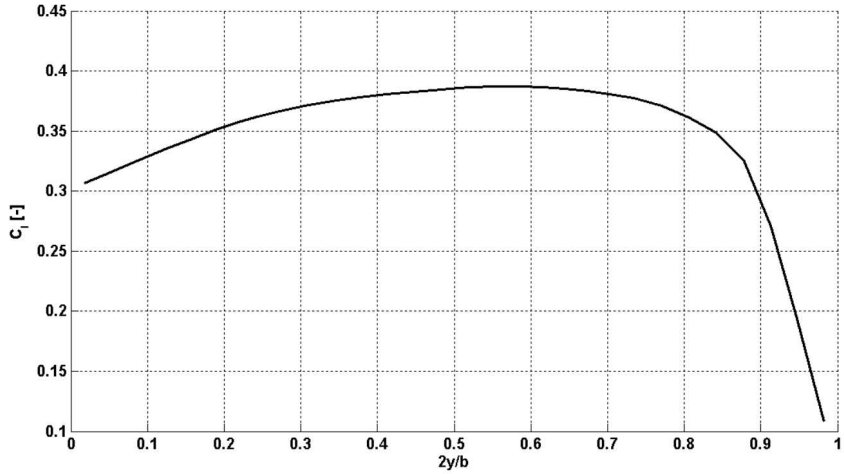

Figure 5.6: Optimized compressible spanwise lift distribution. Lift-constrained isolated wing test case

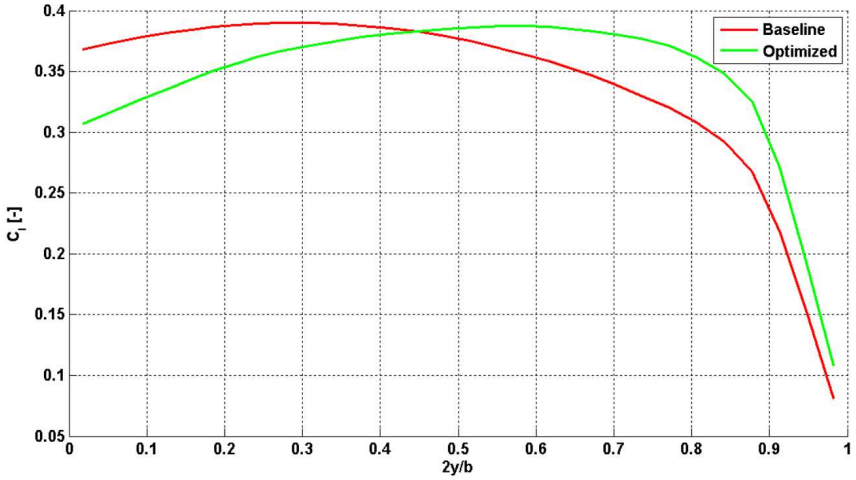

Figure 5.7: Comparison between baseline and optimized spanwise lift distribution. Isolated wing test case

5.2 Target Aircraft rigid wing optimization

In this section we present results for full aicraft rigid optimization.
Just for this optimization we used the gradient enahanced kriging with the initial sampling plan refined with an expected improvement approach something not commonly seen in the literature; with this approach we manage to achieve the optimum with a total of 150 design sites. Gradient of the cost function has been computed with a second order central finite difference scheme: saying that our goal F is a function of the design parameter[5] x_i then the approximation of the

[5] As stated many times, design parameters here are seven local twist angles so that $i = 1 \dots 7$

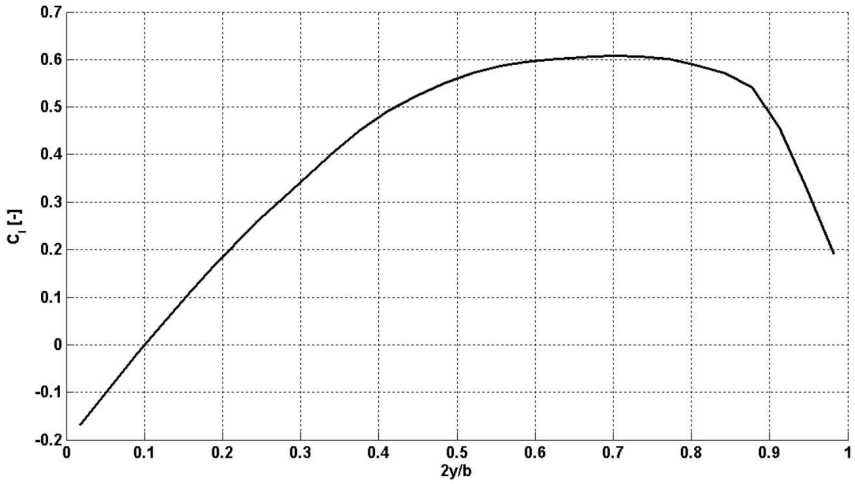

Figure 5.8: Optimized compressible spanwise lift distribution. Lift and pitch-constrained isolated wing test case

cost's function derivative is equation 5.4

$$\frac{\partial F}{\partial x_i} \approx \frac{F\left(x_i + h_i\right) - F\left(x_i - h_i\right)}{2h_i} \tag{5.4}$$

being h_i a small variation in each design parameter; as well known computation of function's derivative by means of finite difference is extremely expensive when the function is expensive to evaluate. Based on equation 5.4, we need $2n+1$ function's evaluation each design sites, n being the number of parameters. Here F is the **trimmed** drag coefficient so that every time we are computing a derivative according to equation 5.4 we actually need to set up two different trim optimization problems 4.6. Having seven design variables means that the computational cost to gather all information necessary to build up the gradient enhanced kriging is that of fifteen trim optimization problems each design site. We can afford this CPU cost here, but when including aeroelasticity in the optimization this will not be true anymore. Beside, the improvement of the gradient enhanced kriging with respect to the simple kriging is not so evident when one needs to compute gradient by means of finite difference for simple kriging approximation with an augmented sampling plan will most likely perform the same as that of a gradient enhanced kriging with a reduced sampling plan but with gradient computed by means of finite difference.
A comparison between the baseline and the optimized rigid wing is reported in table 5.6 and figure 5.9 gives the different spanwise load distribution highlighting once more that a negative sweep wing gives as less drag as possible loading the outer part of the wing while relieving the root, as seen also in figures 5.5 and 5.8.

Being a full aircraft optimization it is interesting to investigate control surfaces' loading, and this is done in figure 5.10.

The main wing gives a slightly smaller contribution to the overall lift coefficient, canards gives almost the same contribution and the optimized configuration uses a lot more horizontal tail than the baseline. The small difference

	$C_{D_{IND}}$	$C_{D_{CFD}}$	$C_{D_{TOT}}$
Baseline	55	101	156
Optimized	53	101	154

Table 5.6: Overall aircraft drag for both the baseline and optimized rigid wing

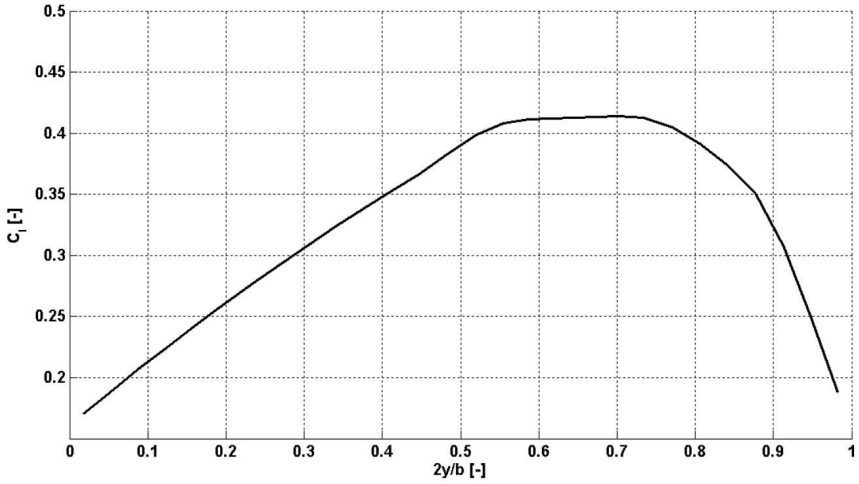

Figure 5.9: Optimum trimmed spanwise lift distribution. Rigid case

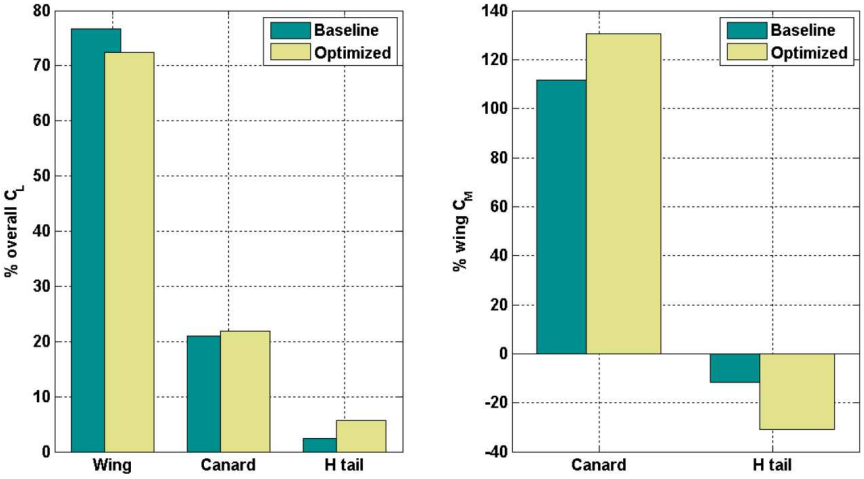

Figure 5.10: Control surfaces loads distribution. Rigid case

in canards' lift gives rise to a significantly higher pitching moment coefficient for the optimized configuration that needs to be counteracted by the horizontal tail increased lift and pitching moment, main wing pitching moment being significantly smaller, see absolute values in table 5.7.

Basically what the optimizer has done is to put as less load as possible on the main wing to reduce the induced drag, and this has been achieved with a

	Baseline	Optimized
$C_{L_{wing}}$	0.3386	0.32
$C_{L_{canard}}$	0.0925	0.0966
$C_{L_{HTail}}$	0.0106	0.025
$C_{M_{wing}}$	-0.4773	-0.4256
$C_{M_{canard}}$	0.5338	0.5578
$C_{M_{HTail}}$	-0.0564	-0.1322

Table 5.7: Three surfaces' load distribution for both the baseline and optimized configurations

lift and pitching moment reduction with respect to the baseline configuration. The lift reduction requires the canard and the horizontal tail to give more lift, pitching moment going along with it.
Comparison between the baseline and the optimized twist spanwise distribution can finally be seen in figure 5.12: it looks like the optimum spanwise twist distribution is parabolic and not linear as in the baseline wing. This behaviour is confirmed for the aeroelastic optimization too, see below.
In order to asses if the gradient enhanced exepcted improvement approach has been successful in its search, and since we just take a few seconds to perform a trimmed-drag evaluation we decided to use a genetic algorithm to search both the true function and its gradient enhanced kriging approximation. The direct search ended up with the same trimmed drag level but a different twist distribution. Kriging evaluation of the direct search optimum's location yielded once more the same drag level, namely those 154 *counts* of table 5.6. Working the other way around the kriging global search gave again the same drag level as above but with another twist distribution. On this basis we conclude that our kriging approximation is **working effectively** and that we have achieved a **flat design space**, see also figure 5.11.

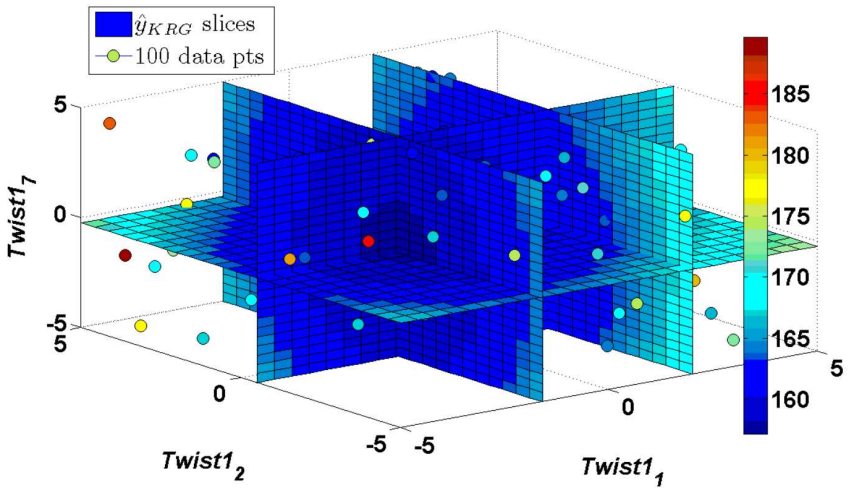

Figure 5.11: Slices of the flat trimmed-drag design space. Contours are in counts. Rigid case

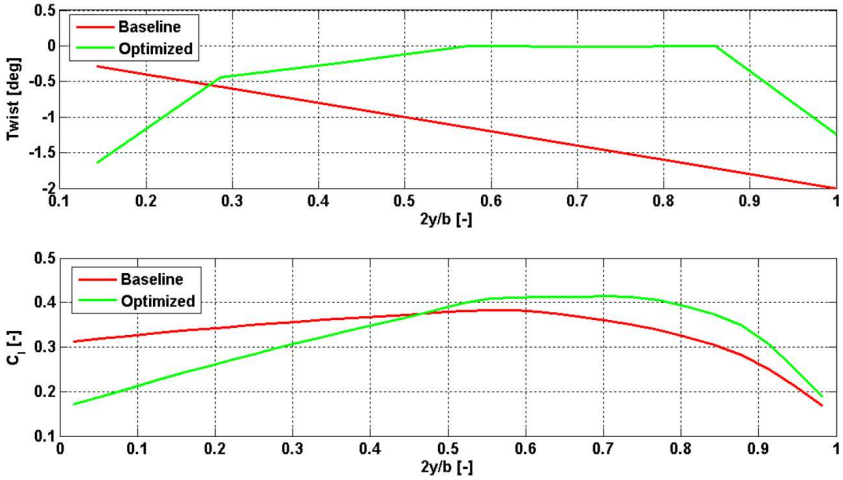

Figure 5.12: Twist and spanwise lift distribution for both the baseline and optimized rigid wings

We will now compare results obtained with our optimization process against full three dimensional CFD evaluations.
We achieved a shock free wing, as in the isolated wing test case, and control surfaces are shock free too, which is important for flight mechanics considerations and confirm that no control surfaces' lift correction was needed. Overall EDGE lift, drag and pitching moment coefficients can be found in table 5.8. These are very good results, but let's look at them in details: lift coefficient is close to the target coefficient but underpredicted for both cases, most likely because we didn't apply any correction to either of the control surfaces, and obviously the pitching moment coefficient goes along with it. Drag coefficient is substantially overpredicted for both configurations, but this is not a real issue because of the same reasone above, namely no correction has been applied to control surfaces so that there's no real business in accurate overall drag prediction. Despite all the approximations involved we have a reasonable trimmed optimized configuration which performs better than the baseline one. It would look like that a count difference in drag is not much: the two CFD results are at the appropriate angle of attack for each configurations[6], but are not at the same lift coefficient, baseline configuration giving less lift and yet giving more drag. This means that at the same lift coefficient it will most likely give more drag, induced drag at least. We have no room here to assess this statement with a CFD solution, for we would need to set up the trim optimization problem 4.6 and that would get too computational intensive; beside a small increment between the optimized and the baseline configuration is seen in the corrected vortex lattice results too: this happens because we used only sections' twist angle as design variables and this probably allows for small improvement as those achieved here.

We go even deeper in analyzing EDGE's results looking at control surfaces' load in table 5.9

Beside the fortuitous lift coefficient match for the baseline wing these results

[6]The angle of attack that results from the trim optimization problem 4.6

	C_L	C_D *counts*	C_M
Baseline	0.4201 (0.4417)	283 (156)	−0.0559 (0)
Optimized	0.4382 (0.4417)	282 (154)	−0.0695 (0)

Table 5.8: EDGE three dimensional results for baseline and optimized configurations, VLM corrected results in parenthesis for ease of comparison

	Baseline	Optimized
$C_{L_{wing}}$	0.3386 (0.3386)	0.3370 (0.32)
$C_{L_{canard}}$	0.0738 (0.0925)	0.0788 (0.0966)
$C_{L_{HTail}}$	0.0077 (0.0106)	0.0224 (0.025)
$C_{M_{wing}}$	-0.4379 (-0.4773)	-0.4076 (-0.4256)
$C_{M_{canard}}$	0.4166 (0.5338)	0.4456 (0.5578)
$C_{M_{HTail}}$	-0.0346 (-0.0564)	-0.1075 (-0.1322)

Table 5.9: EDGE three surfaces' load distribution for both the baseline and optimized configurations, VLM corrected results in parenthesis for ease of comparison

confirm isolated wing test case results of the previous section. Control surfaces lift is a little bit underpredicted and so is the pitching moment, horizontal tail loads being better than canard's loads for the horizontal tail features symmetric airfoil with a twenty degrees sweep at low angle of attack, and in this situation the simple Prandtl-Glauert corrected VLM method gives good approximation to a more advanced CFD solution; nevertheless these are excellent results.

5.3 Target Aircraft wing aeroelastic optimization

Here we present optimization results for the three surfaces' elastic Target Aircraft with a simple kriging on a 750 design of experiments with no expected improvement. We used a second order polynomial mean model with gaussian correlation function to fit the aeroelastic data.
Once the model has been fit we search it with a genetic algorithm, and the optimum found is then checked with a call to the true function to assess accuracy of the kriging prediction.
The kriging has given us good accuracy, however the proposed **jig** twist distribution looks like in figure 5.13. This is clearly an unacceptable twist distribution on a manufacturing basis and its a possible drawback of allowing each twist section to vary independently of all the others. Upon further investigations of the kriging and true function evaluations we found out that this design space is once more flat, see figure 5.16 and we managed to turn this feature to our advantage, changing twist of the fourth spanwise station to a more acceptable value, as can be seen again in figure 5.13: from now on we will refer to the optimized wing meaning the modified optimized wing. Figure 5.15 gives a comparison between the baseline and optimized $1-g$ wing while in figure 5.14 we compare $1-g$ and rigid optimized twist distribution: they look pretty much the same and this suggest that this is really the true optimum twist distribution and highlights

how flat the design space is since the difference between the rigid wing optimization and the aeroelastic optimization is just one count. Comparison with the baseline wing can be found in table 5.10, while control surfaces' loading can be found in figure 5.17 and in table 5.11. One drag count has been lost with respect to the rigid wing optimization, nevertheless the optimized wing still performs better than the baseline. Loads' distribution among canard, horizontal tail and main wing reveals that the optimized wing produces less lift than the baseline as in the rigid case, but between the two optimized wings the elastic one gives significantly less lift, while the two baselines go the other way around. In both the baseline and optimized elastic case canards give more lift than the rigid case; horizontal tail load for the baseline configuration is almost zero while for the optimized wing is higher than in the rigid case.

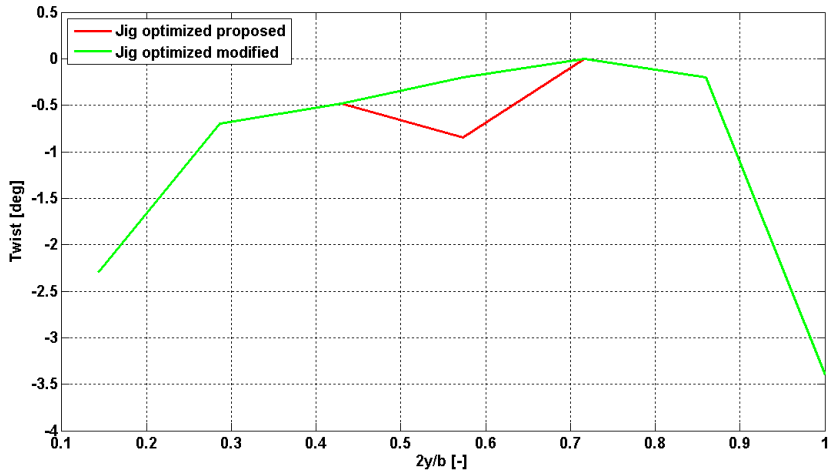

Figure 5.13: Optimizer proposed jig twist distribution and its *modification*

	$C_{D_{IND}}$	$C_{D_{CFD}}$	$C_{D_{TOT}}$
Baseline	54	102	156
Optimized	53	102	155

Table 5.10: Overall aircraft drag for both the baseline and optimized elastic wing

Now we compare these results with three dimensional CFD computations once more. We can basically draw the same conclusion as for the rigid wing comparison, overall CFD coefficients can be found in table 5.12 while control surfaces' loads can be found in table 5.13, however for the elastic case there is a more significant difference between main wing's CFD and corrected-VLM loads.

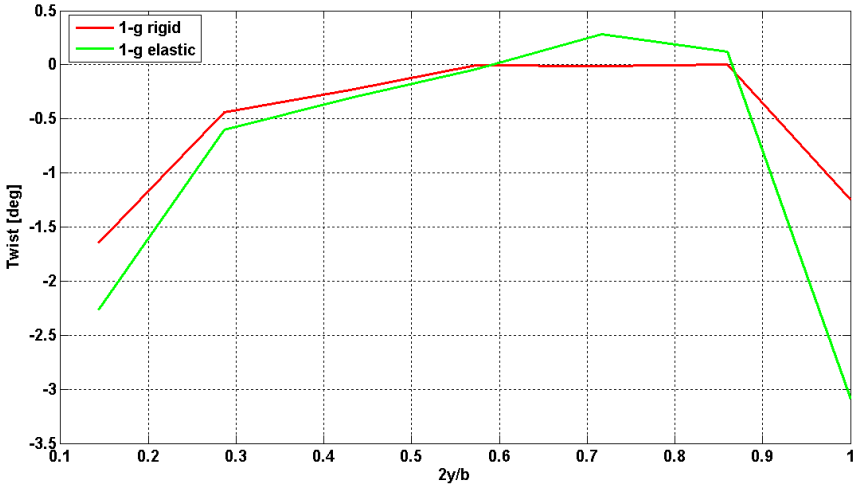

Figure 5.14: Rigid and aeroelastic optimized $1-g$ twist distribution

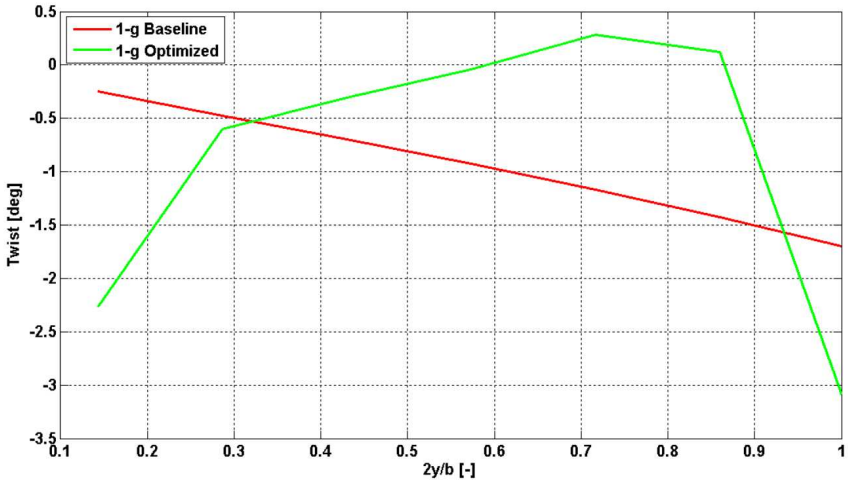

Figure 5.15: Baseline and optimized 1-g twist distribution

	Baseline	Optimized
$C_{L_{wing}}$	0.3506	0.3079
$C_{L_{canard}}$	0.0881	0.1005
$C_{L_{HTail}}$	0.0030	0.0332
$C_{M_{wing}}$	-0.4926	-0.4061
$C_{M_{canard}}$	0.5075	0.5807
$C_{M_{HTail}}$	-0.0162	-0.1758

Table 5.11: Three surfaces' load distribution for both the baseline and optimized aeroelastic configurations

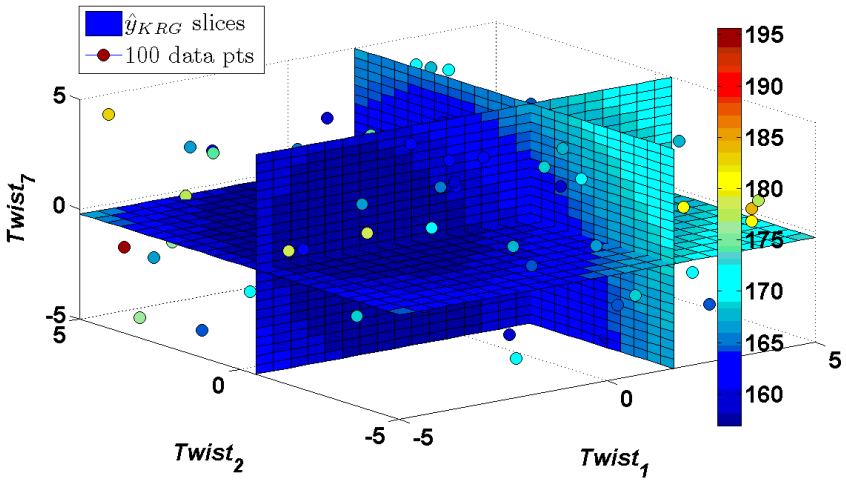

Figure 5.16: Slices of the flat trimmed-drag design space for the elastic wing as function of jig twist. Contours are in counts

	C_L	C_D *counts*	C_M
Baseline	0.4240 (0.4417)	285 (156)	−0.0486 (0)
Optimized	0.4397 (0.4417)	283 (155)	−0.0814 (0)

Table 5.12: EDGE three dimensional results for baseline and optimized aeroelastic configurations, VLM corrected results in parenthesis for ease of comparison

	Baseline	Optimized
$C_{L_{wing}}$	0.3566 (0.3506)	0.3314 (0.3079)
$C_{L_{canard}}$	0.0693 (0.0881)	0.0813 (0.1005)
$C_{L_{HTail}}$	-0.0019 (0.0030)	0.0270 (0.0332)
$C_{M_{wing}}$	-0.4569 (-0.4926)	-0.4121 (-0.4061)
$C_{M_{canard}}$	0.3907 (0.5075)	0.4518 (0.5807)
$C_{M_{HTail}}$	0.0175 (-0.0162)	-0.1211 (-0.1758)

Table 5.13: EDGE Three surfaces' load distribution for both the baseline and optimized configurations, VLM corrected results in parenthesis for ease of comparison

5.4 Target Aircraft wing aerostructural optimization

In this section we present results for a multidisciplinary optimization. We used the same 750 design of experiments of the previous optimization for a structural cost function evaluation **at the same flight speed** as the aerodynamic cost function but at a pull-up load factor of $n_z = 2.5g$: we gathered bending moment and torque data and fit them with a kriging with a first order polynomial mean model and gaussian correlation function. The multidisciplinary optimization is

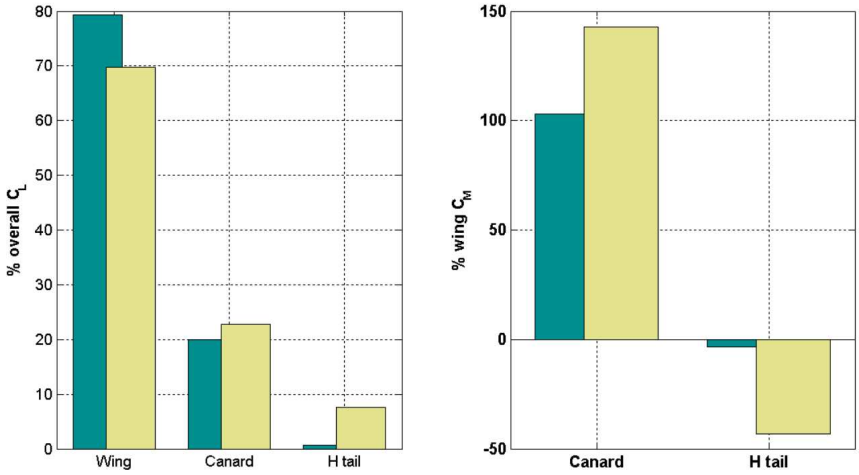

Figure 5.17: Control surfaces loads distribution. Aeroelastic case

then set up with the cost function described in equation 5.5

$$F = w_1 C_D + w_2 abs\left(C_{bending} + C_{torque}\right) \tag{5.5}$$

being w_1 and w_2 two different optimization weights for which hold $w_1 + w_2 = 1$. $C_{bending}$ and C_{torque} are bending moment and torque coefficients defined as in equation 5.6

$$\begin{aligned} C_{bending} &= \frac{M_{bending}}{q_\infty bS} \\ C_{torque} &= \frac{M_{torque}}{q_\infty bS} \end{aligned} \tag{5.6}$$

By varying w_1 weight we perform a trade study between aerodynamics and structures, see figure 5.18; this is just a **preliminary** study, results presented here are by no means definitive. We will be studying this design space deeply in the future but we believe some conclusions can be drawn here as well. Beside, a more formal approach would certainly be that of building a Pareto front [34].

For this optimization we didn't perform any EDGE comparison for we believe results from previous sections have shown enough reliability.

In figure 5.19 we can see spanwise $2.5g$ lift distribution. When the aerodynamics contribution in equation 5.5 is significant the outer part of the wing is loaded most. For the purpose of comparison in figure 5.19 there is also the $2.5g$ pull-up lift distribution for the optimized elastic wing of the previous section. They basically behave the same from an aerodynamic point of view, there is just one count difference, and consequently we believe that we could fix that bumpy behaviour changing the jig twist and exploiting the flatness of the design space as we did before; we believe this will also be true when the structural weight in equation 5.5 increases, but this statement need further investigations.

As the structural weight start to increase, or either the aerodynamic weight start to decrease, the optimizer tends to move the aerodynamic load toward wing root, unloading wing tip.

This behaviour is maximum when $w_1 = 0.25$ so that the aerodynamic part is less significant. Loading the outboard part of the wing rise both the bending

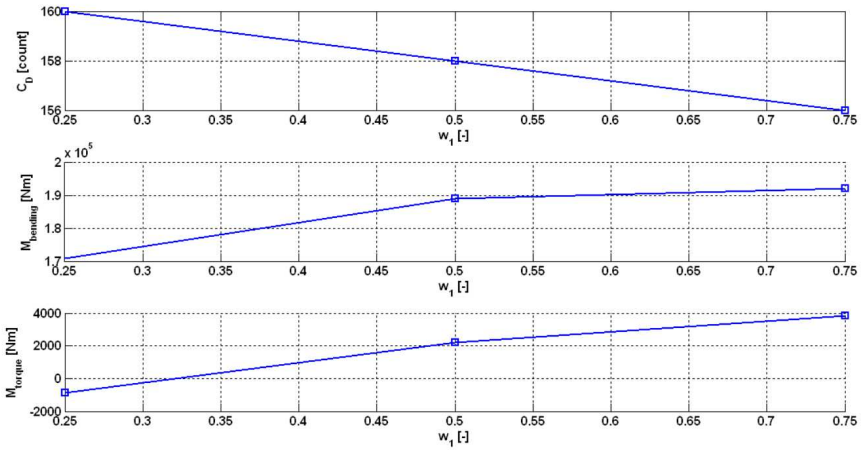

Figure 5.18: Trade study between aerodynamic and structure

and torque moment (the torque moment because of the negative sweep wing) because of the distance between outboard stations and the root. Evidently, aerodynamics and structural needs disagree and a multidisciplinary optimization can help get the best out of both. Indeed while it is evident from figure 5.18 that the lower the bending and torque moment the higher will be the **trimmed drag coefficient** it is also true that bending moment and torque reductions go along with a reduction of wing's weight, hence a reduction of the **trimmed drag coefficient**[7]. Hence there is an evident need for a multidisplinary optimization.

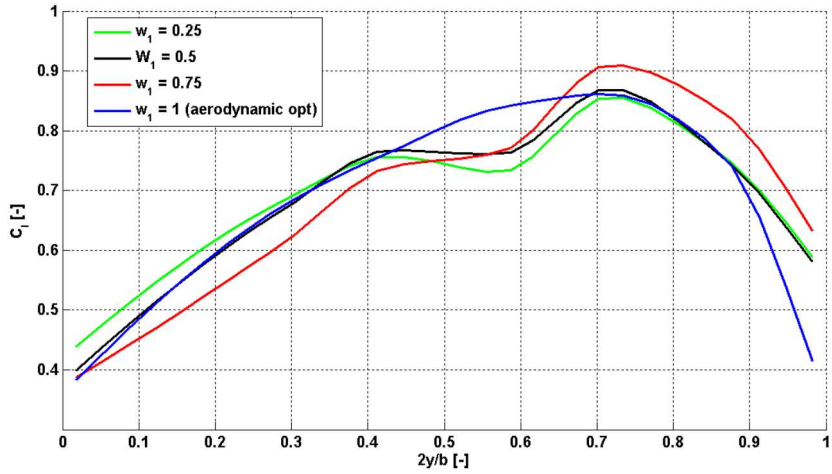

Figure 5.19: Different spanwise main wing 2.5g pull-up lift distribution varying w_1 weight

[7]If aircraft's weight decreases the target lift coefficients in equation 4.6 decreases and the induced drag at least will decrease too

Chapter 6

Conclusions and future works

We presented an aerodynamic optimization procedure intended to be used during early design phases of a transonic aircraft. All goals have been achieved. The need for a fast and computational inexpensive algorithm has been satisfied and Target Aircraft's wing has been optimized in a multidisciplinary environment that included aerodynamics, static aeroelasticity and flight mechanics.
The core of this work is the correction process needed to make the fast vortex lattice method feel the presence of an eventual shock wave. Instead of keeping the VLM AVL code in the loop its main features have been exploited with the extensive use of metamodeling techniques: this significantly reduced the number of actual AVL evaluation and increased the optimizer speed while allowing for a significantly large design space. Exactly the goal we had in mind.
Results from our optimization have been compared with a high fidelity CFD flow solver and they have been found in reasonable good agreement, but, most important, this VLM-corrected optimization procedure can detect coefficients variations in a reasonably accurate way when compared to the high fidelity flow solver, and this has two major consequences:

- it can be used in a preliminary aerodynamic design environment to explore a large number of very different configurations
- it can be used in a multifidelity multidisciplinary optimization process as a low fidelity model. The use of the multifidelity kriging is suggested since this approach is finding its way through the design process [21, 35, 44, 55]. If relying only upon computational methods I would like to suggest a multifidelity gradient enhanced kriging, because of the very good performance of gradient enhance kriging found here and in the literature.

This tool can be effectively used both to trim the aircraft and to evaluate its trimmed drag for aerodynamic shape optimization: this particular point has been another novel idea of the present work, for aircraft trim has usually been considered to evaluate aircraft load, while here has been used both for aerodynamics and structural purposes.
Despite all this a more torough comparison between this low fidelity and the high fidelity CFD models should be carried out with a grid convergence study

on each configuration tested, but this subject has not been pursued any further here because of the limited computational resources available. Regarding the achieved results those small improvement seen are most likely due to the nature of the design variables and their limited number. As a future work one should also allow two dimensional airfoil shape to vary, and in that case we believe there will be a much higher improvement once the optimization has been completed. The optimum spanwise trimmed lift distribution is seen to load wing tips much more than wing root and is not elliptic as one might expect: isolated wing incompressible and compressible lift and pitch constrained optimization confirmed this behaviour. The distance of each wing section to the center of gravity should be considered as an explanation. This load distribution is undesirable from an airworthiness point of view for at high angles of attack wing tip will likely stall before the root and might lead to premature shock stall or buffet when the load is increased at high speed [32]. In a possible future work it might be interesting to add a lift-distribution penalty term to the aerodynamic optimization, something as in equation 6.1 should suffice,

$$F_{stall} = \frac{1}{2}\int_y (C_l - C_{l_d})^2 \tag{6.1}$$

This is a modified version of an inverse design cost function as proposed by Jameson in [32] and C_{l_d} is the desired lift coefficient distribution that is intended to be used in the current framwork; when reverting to the use of high fidelity CFD models lift coefficient distribution should be replaced by pressure distribution.
With the stall issue in mind it should be also considered that if the canard stalls before the wing then it will give rise to a nose down pitching moment that will reduce the angle of attack and prevent the wing to reach its stall angle, while still having the horizontail tail to provide for additional control. This could be another possible advantage of a three surface aircraft, but this subject needs to be investigated further with high fidelity models in a multidisciplinay environment that includes, at least, both aerodynamics and flight mechanics, something that has never been done yet.
Both the rigid and the elastic optimizer gave almost the same $1-g$ twist distribution and this suggest that the true optimum has indeed been reached. A flat design space has been found: we are under the impression that the correction process is responsible for this, but it is also known that aerodynamic design spaces are indeed flat, see Jameson [32, 6, 4].
The aerostructural optimization needs further investigation so that a Pareto front can be built and trade studies can be performed, here we just scratched the surface of it. However it is evident that aerodynamic and structure have different needs and it is appropriate to keep into account both in an aircraft design environment. In the future we also plan to add an handling qualities term to our multidisciplinary cost function.
Regarding the optimization techniques used I agree with the well knwon saying that there's no final optimization algorithm, each problem has its own need and must be treated consequently; also each optimization algorithm has its own advantage and disadvantage that need to be taken into account. However the use of metamodeling techqniques leaves more freedom to the designer an feed him/her with much more information about the design space that can be appropriately exploited.

As a final warning we conclude that those good results achieved above have been facilitated by the low sweep Target Aircraft's wing: the tool developed here should be tested on a higher sweep wing too. We expect its results to deteriorate because of more pronounced three dimensional effects, but it should be capable of giving reasonably accurate results again.
As a ultimate goal one can set the minimization of trimmed drag of the aeroelastic aircraft in a high fidelity environment in a reasonable amount of time, something we believe can be achieved with extensive use of metamodeling again.

Bibliography

[1] L T Watson A A Giunta. A comparison of approximation modeling techniques: polynomials versus interpolating models. *AIAA*, (4758), 1998.

[2] L Riccobene A Scotti A De Gaspari, S Ricci. Active aeroelastic control over a multisurface wing: modeling and wind tunnel testing. *Journal of aircraft*, 47(9), 2009.

[3] A J Keane A I J Forrester. Recent advances in surrogate based optimization. *Progress in aerospace sciences*, (45), 2009.

[4] S Shankaran A Jameson, J C Vassberg. Aerodynamic-structural design studies of low-sweep transonic wings. *AIAA*, (145), 2008.

[5] N Quin A Vavalle. Iterative response surface based optimization scheme for transonic airfoil design. *Journal of aircraft*, 44(2), 2007.

[6] N Harrison A Jamenson D Roman J Vassberg B Epstein, S Peigin. Comparative study of 3d wing drag minimization by different optimization techniques. *AIAA*, (326), 2008.

[7] J E Bussoletti B M Kulfan. Fundamental parametric geometry representations for aircrafts component shapes. *AIAA*, (6948), 2006.

[8] W H Mason B Malone. Multidisciplinary optimization in aircraft design using analytic technology models. *AIAA*, (54093), 1991.

[9] A J Booker. Design and analysis fo computer experiments. *AIAA*, (4757), 1998.

[10] T F Wunderlich C M Liersch. A fast aerodynamic tool for preliminary aircraft design. *AIAA*, (5901), 2008.

[11] J.J. Alonso H.S. Chung. Using gradients to construct cokriging approximation models for high-dimensional design optimization problems. *AIAA*, (0317), 2002.

[12] E N Tinoco M Mani O P Brodersen B Eisfeld R A Whals J H Morrison T Zickuhr D Levy M Murayama D J Mavriplis, J C Vassberg. Grid quality and resolution issues from the drag prediction workshop series. *Journal of aircraft*, 46(3), 2009.

[13] W A Crossley D P Raymer. Variations of genetic algorithm and evolutionary methods for optimal aircraft sizing. *AIAA*, (5839), 2002.

[14] W J Welch D R Jones, M Schonlau. Efficient global optimization of expensive black box function. *Journal of global optimization*, 13, 1998.

[15] I Kroo D Rajnarayan, A Haas. A multifidelity gradient-free optimization method and application to aerodynamic design. *AIAA*, (6020), 2008.

[16] L T Watson F A C Viana, R T Haftka. Why not run the efficient global optimization algorithm with multiple surrogates? *AIAA*, (3090), 2010.

[17] V Steffen Jr F A C Viana, R T Haftka. Multiple surrogates: how cross-validation errors can help us to obtain the best predictor. *Structural and multidisciplinary optimization*, (39), 2009.

[18] P Hajela. Nongradient methods in multidisciplinary design optimization, status and potential. *Journal of aircraft*, 36(1), 1999.

[19] J. Himisch. Winglet shape and load optimization with a numerically supported lifiting line method. *AIAA*, (5902), 2008.

[20] C Werner-Westphal W. Heinze P. Horst. Improved representation of high lift devices for a multidisciplinary preliminary aircraft design process. *AIAA*, (5872), 2008.

[21] E Leonardi I T Watson, T J Barber. Validation of numerical and experimental results using the kriging estimator. *AIAA*, (3301), 2006.

[22] D H Lee O H Rho J Ahn, H J Kim. Response surface method for airfoil design in transonic flow. *Journal of aircraft*, 38(2), 2001.

[23] J J Alonso M J Rimlinger D Saunders J J Reuther, A Jameson. Constrained multipoint aerodynamic shape optimization using an adjoint formulation and parallel computers, part 1. *Journal of aircraft*, 36(1), 1999.

[24] J J Alonso M J Rimlinger D Saunders J J Reuther, A Jameson. Constrained multipoint aerodynamic shape optimization using an adjoint formulation and parallel computers, part 1. *Journal of aircraft*, 36(1), 1999.

[25] A Plotkin J Katz. *Low speed aerodynamics - From wing theory to panel methods*. Mc Graw Hill, 1991.

[26] A Plotkin J Katz. *Low speed aerodynamics*. Cambridge University Press, 2001.

[27] M Meaux J Laurenceau. Comparison of gradient and response surface based optimization frameworks using adjoint methods. *AIAA*, (1889), 2008.

[28] P Sagaut J Laurenceau. Building efficient reponse surfaces of aerodynamic functions with kriging and cokriging. *AIAA Journal*, 46(2), 2008.

[29] J E Cooper J R Wright. *Introduction to aircraft aeroelasticity and loads*. Wiley, 2007.

[30] T J Mitchell H P Wynn J Sacks, W J Welch. Design and analysis of computer experiments. *Statistical sciences*, 4(4), 1989.

[31] A Jameson. Optimum aerodynamic design using cfd and control theory. *AIAA*, (36580), 1995.

[32] A Jameson. A perspective on computational algorithms for aerodynamic analysis and design. *Progress in aerospace sciences*, (37), 2001.

[33] K Nakahashi H Morino K Chiba, S Obayashi. High-fidelity multidisciplinary design optimization of aerostructural wing shape for regional jet. *AIAA*, (5080), 2005.

[34] A Jameson K Leoviriyakit S Kim. Aerostructural wing planform optimization using the navier stokes equations. *AIAA*, (4479), 2004.

[35] A. Forrester A. Sobester A. Keane. *Engineering design via surrogates.* Wiley, 2008.

[36] A J Keane. Wing optimization using design of experiment, kriging model and data fusion methods. *Journal of aircraft*, 40(4), 2003.

[37] N. Petruzzelli A. Keane. Wave drag estimation for use with panel codes. *Journal of aircraft*, 38(4), 2001.

[38] E R Kendall. The aerodynamics of three surface airplanes. *AIAA*, (2508), 1984.

[39] E R Kendall. The minimum induced drag, longitudinal trim and static longitudinal stability of two surface and three surface aircraft. *AIAA*, (2164), 1984.

[40] E R Kendall. Performance trades of two surface and three surface configurations. *AIAA*, (2221), 1984.

[41] B M Kulfan. Universal parametric geometry representation method. *Journal of aircraft*, 45(1), 2008.

[42] S. Ricci M.Terraneo. Conceptual design of an adaptive wing for a three-surfaces airplane. *AIAA*, (1959), 2005.

[43] W Shyy T Goel R Vaidyanathan P K Tucker N V Queipo, R T Haftka. Surrogate based analysis and optimization. *Progress in aerospace sciences*, (41), 2005.

[44] A. Keane P. Nair. *Computational Approaches for aerospace design.* Wiley, 2005.

[45] S Guillemot M Henshaw A Karlsson V Selimin J Smith E Teupootahiti B Winzell P. G. Lavigne, J P Grisval. Comparison of static and dynamic fluid structure interaction solutions in the case of a highly flexible modern transport aircraft wing. *Aerospace science and technology*, (7), 2003.

[46] S Kim R Mukherjee, A Gopalarathnam. An iterative decambering approach for post stall prediction of wing characteristics using knwon section data. *AIAA*, (1097), 2003.

[47] D P Raymer. *Aircraft design: a conceptual approach.* AIAA education series, 2006.

[48] A Scotti S Ricci. Gust response alleviation on flexible aircraft using multi-surface control. *AIAA*, (3117), 2010.

[49] J Cecrdle J Malecek S Ricci, A Scotti. Active control of three surface aeroelastic model. *Journal of aircraft*, 45(3), 2008.

[50] O. Gur W. Mason J. Schetz. Full-configuration drag estimation. *Journal of aircraft*, 47(4), 2010.

[51] W Shyy N V Queipo T Goel, R T Haftka. Ensemble of surrogates. *Structural and multidisciplinary optimization*, (33), 2007.

[52] T M Mauery F Mistree T W Simpson, J J Korte. Comparison of response surface and kriging models for multidiscplinary design optimzation. *AIAA*, (4755), 1998.

[53] FAC Viana. *SURROGATES Toolbox User Guide*. http://sites.google.com/site/fchegury/surrogatestoolbox, 2010.

[54] D J Mavriplis W Yamazaki, M P Rumpfkeil. Design optimization utilizing gradient hessian enhanced surrogate model. *AIAA*, (4363), 2010.

[55] S Gortz Z H Han, R Zimmermann. A new cokriging method for variable-fidelity surrogate modeling of aerodynamic data. *AIAA*, (1225), 2010.